Towards Estimation of Seasonal Water Dynamics of Winter Wheat from Ground-Based L-Band Radiometry: a Concept Study

Thomas Jagdhuber[1,2], François Jonard[3,4], Anke Fluhrer[1,2], David Chaparro[5], Martin J. Baur[6], Thomas Meyer[4] and María Piles[7]

[1] German Aerospace Center, Microwaves and Radar Institute, Münchener Strasse 20, 82234 Wessling, Germany
[2] Institute of Geography, University of Augsburg, Alter Postweg 118, 86159 Augsburg, Germany
[3] Geomatics Unit, Université de Liège (ULiege), Allée du Six Août 19, 4000 Liège, Belgium
[4] Agrosphere (IBG-3), Institute of Bio- and Geosciences, Forschungszentrum Jülich GmbH, 52428 Jülich, Germany
[5] Universitat Politècnica de Catalunya, CommSensLab & IEEC/UPC, Jordi Girona 1-3, 08034 Barcelona, Spain
[6] University of Cambridge, Department of Geography, Philippa Fawcett Dr, CB3 0AS, Cambridge, U.K.
[7] Image Processing Lab, Universitat de València, 46980 Valencia, Spain

Correspondence to: Thomas Jagdhuber (Thomas.Jagdhuber@dlr.de), Tel.: +49-8153-28-2329

Abstract. The vegetation optical depth (VOD) variable contains information on plant water content and biomass. It can be estimated alongside soil moisture from currently operating satellite radiometer missions, such as SMOS (ESA) and SMAP (NASA). The estimation of water fluxes, such as plant water uptake (PWU) and transpiration rate (TR), from these earth system parameters (VOD, soil moisture) requires assessing potential (suction tension) gradients of water and flow resistances in the soil, the vegetation and the atmosphere. Yet water flux estimation remains an elusive challenge especially on a global scale. In this concept study, we used a field-scale experiment to test mechanistic models for the estimation of seasonal water fluxes (PWU and TR) of a winter wheat stand including measurements of soil moisture, VOD, and relative air humidity (RH) under a controlled environment. We utilized microwave L-band observations from a tower-based radiometer to estimate VOD of a wheat stand during the 2017 growing season at the Selhausen test site in Germany. From VOD, we first extracted the gravimetric moisture of vegetation and then determined the relative water content (RWC) and vegetation water potential (VWP) of the wheat field subsequently. Although the relative water content could directly be estimated from VOD, our results indicate this may be challenging for the phenological phases, when rapid biomass and plant structure development take place within the wheat canopy. The water uptake from the soil to the wheat plants was estimated from the difference between the soil and vegetation potentials divided by the flow resistance from soil into wheat plants. The transpiration rate from the wheat plants into the atmosphere was obtained from the difference between the vegetation and atmosphere potentials divided by the flow resistances from plants to the atmosphere. For this, the required soil matric potential (SMP), the vapor pressure deficit and the flow resistances were obtained

from on-site observations of soil, plant and atmosphere together with simple mechanistic models. This pathfinder

35 study shows that the L-band microwave radiation contains valuable information on vegetation water status that enables the estimation of water dynamics (up to fluxes) from the soil via wheat plants into the atmosphere, when combined with additional information of soil and atmosphere water content. Still, assumptions have to be made when estimating the vegetation water potential from relative water content as well as the water flow resistances between soil, wheat plants and atmosphere. Moreover, direct validation of water flux estimates for the assessment

40 of their absolute accuracy could not be performed due to a lack of in situ PWU and TR measurements. Nonetheless, our estimates of water status, potentials and fluxes show the expected temporal dynamics, known from literature, and intercompare reasonably well in absolute terms with independent TR estimates of the NASA ECOSTRESS mission, providing confidence in further developing the proposed approach. Our findings support that passive microwave remote sensing techniques qualify for the estimation of vegetation water dynamics next to

45 traditionally measured stand-scale or plot-scale techniques. They might shed light on the potential capabilities of monitoring water dynamics in the soil-plant-atmosphere system including wide-area, remote sensing-based earth observation data.

1 Introduction

50 The monitoring of water dynamics between soil, vegetation and atmosphere and therefore the water availability for plants requires a system-driven and holistic approach integrating the three water storage compartments. The soil-plant-atmosphere system (SPAS) represents such an approach, linking the water, energy and carbon cycles (Reichardt and Timm, 2014; Manzoni et al., 2013a; Ritchie, 1981; Cowan, 1965). SPAS is understood as a physical continuum, in which water dynamics occur as interdependent transfer processes between the three system

55 compartments (Nobel, 2020). Gardner (1960; 1965) was among the first to study the system holistically and to point out that the water in the system flows in the direction of decreasing energy leading to the concept of water potential in soil, plant and atmosphere (Slayter & Taylor, 1960). A gradient in water potential induces a flow, for instance, from soil via roots and plant parts into the atmosphere decelerated by the resistance of the traversed system compartments (Oosterhuis and Walker, 1987; Choudhury and Idso, 1985; Yan and Jong, 1971).

60 The water potential (WP) refers to the potential energy of water and is a key variable in plant physiology (Reichardt and Timm, 2014). Since plants are the central component of the SPAS, the decreasing gradient in WP from soils to the atmosphere drives the movement of water through plants (Elfving et al., 1972; Pearcy et al., 2012). Thus,

the vegetation water potential (VWP) changes according to the water availability in soils and the uptake capabilities of the plant root and xylem systems, according to the regulation of transpiration through the stomata in leaves, and according to the vapor pressure deficit in the atmosphere (Lambers et al., 2008; Jonard et al., 2020).

The water transport through the different compartments of the SPAS is coordinated by adaption of potentials and resistances, in a way that water transport and water use efficiency are maximized by the plants, avoiding high-resistance conditions with plant-damaging water potential drops (Tyree and Zimmermann, 2013). According to Manzoni et al. (2014), the coordinated behavior is an outcome of plant adaption to their habitat by optimizing water use and gain in carbon assimilation for plant growth.

Under drought conditions, VWP changes due to a differing water transport through the plant, mainly regulated by stomata closure (Choat et al., 2018; Johnson et al., 2018). Hence, VWP is linked to the regulation of water transport and storage within plants (isohydric to anisohydric behavior) and thereby mechanistically relates key processes in the water, energy and carbon cycles (Lambers et al., 2008; Martinez-Vilalta and Garcia-Forner, 2017). In particular, estimating VWP from satellites would be interesting for regional and global ecological studies addressing drought impacts, especially on forest and agricultural ecosystems (e.g. Feldman et al., 2020). Such retrievals could inform or update global vegetation, earth system, or atmospheric boundary layer models (Bonan et al., 2014; Matheny et al., 2017; Moment et al., 2017; Momen and Bou-Zeid, 2017).

Microwave remote sensing retrieval approaches up to satellite observation missions (e.g. SMOS (ESA) or SMAP (NASA)) often deal with the estimation of earth system parameters (like soil moisture) rather than with the assessment of dynamic flow processes, like water uptake or transpiration of plants (Entekhabi et al., 2010; Kerr et al., 2010; Portal et al., 2020). An exception in terms of estimation of water dynamics is the GRACE mission (Sadeghi et al., 2020a), assessing total water storage change, and especially its combination with the SMOS and SMAP missions (Sadeghi et al., 2020b). The estimation of water dynamics from remote sensing requires assessing the potential (suction tension) gradients of water rather than the (storage) filling status of soils or plants with water. Passive microwave remote sensing techniques should be capable of obtaining VWP-estimates, provided that plant hydraulic trait information is available (Konings et al., 2019). To do so, the vegetation optical depth (VOD) parameter, that measures the degree of attenuation of microwaves as they pass through vegetation, needs to be first extracted from the radiometer observations by model-based parameter retrievals. Afterwards the biomass and water contributions to the VOD parameter need to be disentangled (Martinez-Vilalta et al., 2019). As proposed in Bonan et al. (2014), the relative water content (RWC) can be a valid metric for plant water status and can be utilized to estimate VWP. Konings et al. (2019) explained how microwave remote sensing can be applied for monitoring of

plant parameters, like RWC. In addition, Rao et al. (2019) showed that VOD from X-band satellite radiometry can be converted into RWC-estimates with the caveat that both, water and biomass, influence the VOD especially in seasonally growing agricultural species, like winter wheat. Therefore, only periods with constant biomass should be evaluated in order to isolate the water component directly from VOD. Fink et al. (2018) found a way to extract the gravimetric moisture of vegetation (m_g) from the VOD-signal. m_g can be converted into RWC and is not affected by biomass dynamics. The m_g-estimation methodology of Fink et al. (2018) was further developed and validated at the field-scale in Meyer et al. (2019).

100 For the present study, the dataset of Meyer et al. (2019) is used to estimate water potential and water flux along SPAS for the 2017 growing season of a winter wheat field. This wheat monoculture has the advantage that growth stages between individual plants are nearly completely synchronized and the canopy develops very homogenously. The benefit here is that measurements of individual plants are very likely representative for all other plants and can be scaled to the whole canopy. Most notably, a main motivation for analyzing wheat comes from its importance

105 for food production being one of the major crop types cultivated around the globe.

The winter wheat field was monitored with the ground-based L-band radiometer instrument ELBARA-II. Simultaneously, in situ measurements for key plant (e.g. m_g, height, biomass, leaf area index (LAI), and phenology), soil (e.g. relative permittivity and moisture) and atmosphere (e.g. air temperature, wind speed, net radiation and relative humidity) properties were recorded directly at or around the test field.

110 The objective of this concept study is to research the feasibility of estimating potentials and seasonal flux rates of water (water uptake from soil and transpiration rates into the atmosphere) within the SPAS of a winter wheat field from ground-based L-band radiometry and on-site measurements of soil and atmosphere. With our research we aim to shed light on whether the combination of L-band radiometry and a confined set of on-site measurements are sufficient for the derivation of reasonable water potential dynamics and water flux rates in the SPAS of a winter

115 wheat field.

2 Test site and experimental data

The research study was carried out at the Selhausen remote sensing field laboratory, Germany (Jonard et al., 2015; Jonard et al., 2018). In 2017 winter wheat (*Triticum aestivum L.*) was grown in the crop rotation of the farmers at

120 the field laboratory. Key developmental stages of winter wheat are published by Bruns & Croy (1983) and indicate that this agricultural crop has a distinct phenological cycle in the yearly growing period. Detailed information on

distribution, botany, growth and physiology of winter wheat are presented in Curtis et al. (2002). The winter wheat at Selhausen grew well without irrigation or fertilization. It was also not affected by plant diseases.

The experimental setup, considered in this study, consists of a 12 [m] x 20 [m] plot covered by a mesh reflector (metal grid) on the ground with winter wheat plants growing through it. L-band (1.4 [GHz]) passive microwave measurements were performed using an ELBARA-II radiometer of Forschungszentrum Jülich (FZJ) fixed at 4 [m] height. ELBARA-II features a dual-mode conical horn antenna with an absolute accuracy of 1 [$°K$] and relative sensitivity of < 0.1 [$°K$] (Meyer et al., 2018). Radiometer measurements were repeated twice a week at incidence angles between 40° and 60° in 5° increments.

Solely the vegetation microwave radiation is measured using a mesh reflector on the ground and the radiation from the soil is blocked by the reflector (Jonard et al., 2015). In situ measurements of soil texture (silt loam with 13 [%] sand, 70 [%] silt, and 17 [%] clay), soil permittivity and soil temperature were obtained every 15 [min] (and every 30 [min]) using 15 capacitance sensors installed at 5 [cm] (and using 30 time-domain reflectometry (TDR) sensors installed at 30 [cm]) depth in direct vicinity of the radiometer footprint within the field. Soil permittivity measurements can be converted to soil moisture θ according to the well-established dielectric mixing model of Topp et al., (1980). Precipitation, net solar radiation, air temperature, wind speed and relative humidity data are available in 10 [min]-resolution (except for wind speed at 30 [min]-resolution) from two TERENO climate station, located next to the field laboratory (6.449° E, 50.869° N) and on a neighboring field (6.447° E, 50.865° N). In order to be less dependent on in situ measurements, L-band radiometer-derived soil moisture data could also have been used from a non-meshed area of the winter wheat field instead of the in situ soil permittivity measurements. However, the in situ data have a significantly higher temporal resolution than the radiometer observations. But similar to the soil permittivity, these data could be derived from remote sensing-based approaches in a future, more in situ-independent and larger-scale research study.

Vegetation height [m], leaf area index (LAI) [$m²/m²$], above ground biomass (AGB) [$kg/m²$], and vegetation water content (VWC) [$kg/m²$] were measured destructively every week around the radiometer measurements for comparison and validation. After Meyer et al. (2019), in situ measured VWC was used to obtain in situ m_g by calculating first the dry matter fraction (m_d) as defined by Mätzler (1994), i.e., $m_d= dry\ mass/\ fresh\ mass$, and subtracting it afterwards from one (i.e., $m_g= 1 - m_d$).

All vegetation-related measurements of the growing season in 2017 and the different phenological phases are presented in Figure 1 and Table 1 showing a distinct correlation between VWC and LAI (R=0.94). For a detailed

description of the trends and dynamics of these on-site measurements as well as a full sketch of the experimental setup, the reader is referred to Meyer et al. (2018) and Meyer et al. (2019).

Table 1: Overview of growth stages of the winter wheat between 10th of April (DOY 100) and 14th of August 2017 (DOY 226) and their corresponding phenological phase (after BBCH (*Biologische Bundesanstalt, Bundessortenamt und CHemische Industrie*) code) (Meyer et al., 2018).

155

DOY 2017	Growing stage	BBCH code
100	Tillering	26
108 - 122	Stable stem elongation	30
128 - 142	Further stem elongation (increased plant growth rate)	35
142 - 149	50 % of inflorescence visible	55
157	Beginning of flowering	61
163	Grain development started	71
180	Grain fully developed and start of ripening process	77 and 83 - 89
190 - 226	Early senescence until late senescence	92 -99
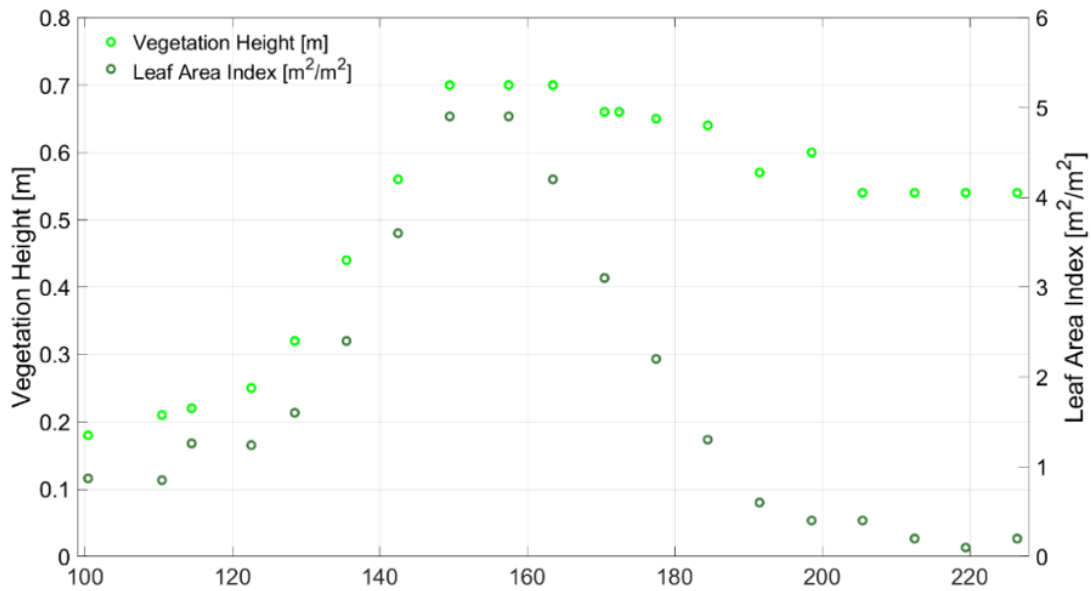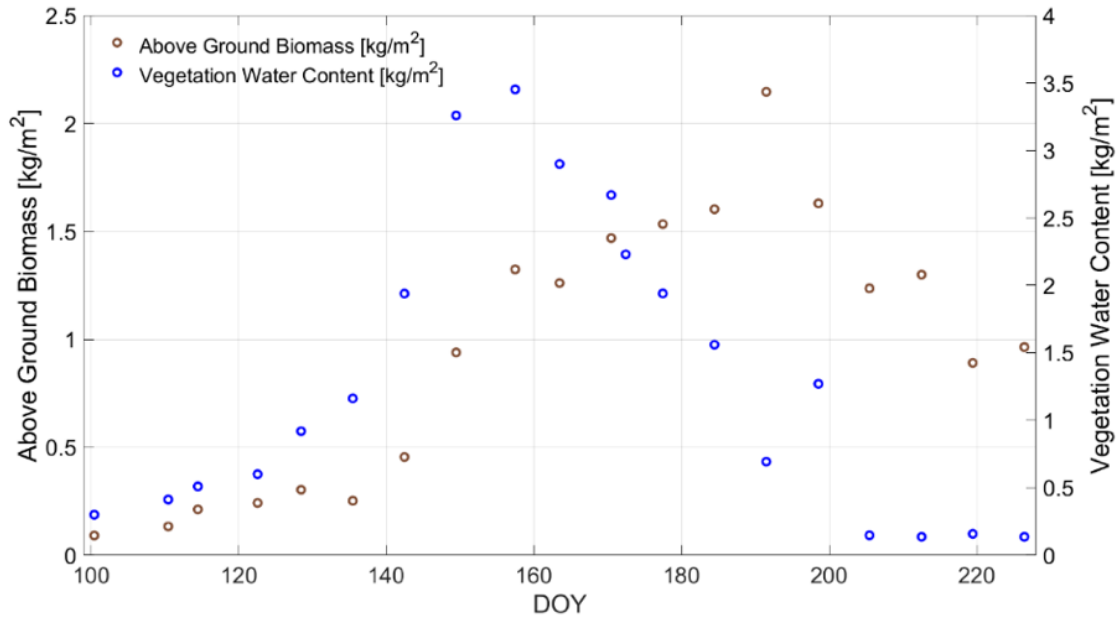
Figure 1: In situ measurements of the wheat field along growing season for days of year (DOY) in 2017 at the Selhausen field laboratory, Germany: Vegetation height [*m*] & leaf area index (*LAI*) [*m²/m²*] (top); above ground biomass (*AGB*) [*kg/m²*] & vegetation water content (*VWC*) [*kg/m²*] (bottom) (Meyer et al., 2018).

160

For later comparison of the transpiration estimates in Selhausen with benchmark information, we apply data from the NASA ECOsystem Spaceborne Thermal Radiometer Experiment on Space Station (ECOSTRESS) mission (https://ecostress.jpl.nasa.gov/). The ECOSTRESS mission was launched in 2018 and carries on board a thermal infrared radiometer with high spatial resolution (70 m). This is used to estimate the earth's surface temperatures and to derive evapotranspiration (*ET*). Two ECOSTRESS L3 products provide ET data: the L3_ET_PT-JPL product, based on L2 information, and the L3_ET_ALEXI product, based on the ALEXI/disALEXI algorithm. In our case, we focus on the L3_ET_PT-JPL product, which also uses MOderate resolution Imaging Spectroradiometer (MODIS) data as auxiliary information and leads to partitioning of *ET* into canopy transpiration and soil evaporation (Halverson et al., 2019).

We compare our transpiration estimates in Selhausen (2017) with ECOSTRESS L3_ET_PT-JPL transpiration data for years 2019, 2020 and 2021, for DOY between 100 and 200. Note that no ECOSTRESS data is available for this DOY period in 2018, and that the number of data available varies for each year and is irregularly distributed, which hinders obtaining regularly sampled time series. The L3_ET_PT-JPL dataset provides instantaneous information (i.e., transpiration at MODIS time over pass: 10.30 a.m. local time, approximately) and daily information (i.e., a daily integral of *ET* built from a sinusoidal model mimicking radiation intensity; Halverson et al., 2019). Uncertainty information is available for the instantaneous *ET* dataset: when uncertainty was higher than 50% of the transpiration value, we excluded the respective date. In addition, note that nightly overpasses of

the ECOSTRESS sensor are excluded. Moreover, transpiration estimates equal to zero are screened out due to unlikely (probably wrong) 100% vs. 0% partition of ET (between soil evaporation and canopy transpiration respectively). Finally, at some days two or more transpiration estimates are available. Thus, we compute the median for each day to ensure we finally have one transpiration estimate per day. Transpiration estimates of L3_ET_PT-JPL are in units of [W/m^2]. We transform these estimates into units of [mm/s] as follows (Halverson et al., 2019): $TR\left[\frac{mm}{s}\right] = TR\left[\frac{W}{m^2}\right] \cdot 10^{-6} \cdot LH$ where LH is latent heat and is computed with $LH = 2.501 - 0.002361 \cdot T$. T is temperature in degree Celsius. T is obtained in 30-minutes timesteps from a meteorological station next to the Selhausen test field. For the instantaneous transpiration data, T at 10:30 a.m. is used. For the daily transpiration data, T is averaged between 7 a.m. and 8 p.m..

3 Methodology of water dynamics estimation

The methodology for water dynamics estimation - water uptake from soil to wheat vegetation (PWU) & transpiration from wheat vegetation to atmosphere (TR) - is conceptualized in the workflow of Figure 2. First, the water status of soil (θ), vegetation (m_g; cf. section 2) and atmosphere (RH) need to be known from remote sensing estimates or on-site measurements. From the water status, the water potentials for the three environmental compartments (soil, vegetation & atmosphere) are calculated (sections 3.1 to 3.3) and then SMP and VWP are used to retrieve the water uptake from the soil into the wheat vegetation (section 3.4). In addition, the atmospheric water potential, usually expressed by the vapor pressure deficit (VPD), is applied together with the VWP to calculate the transpiration rate of the wheat vegetation into the atmosphere (section 3.5).
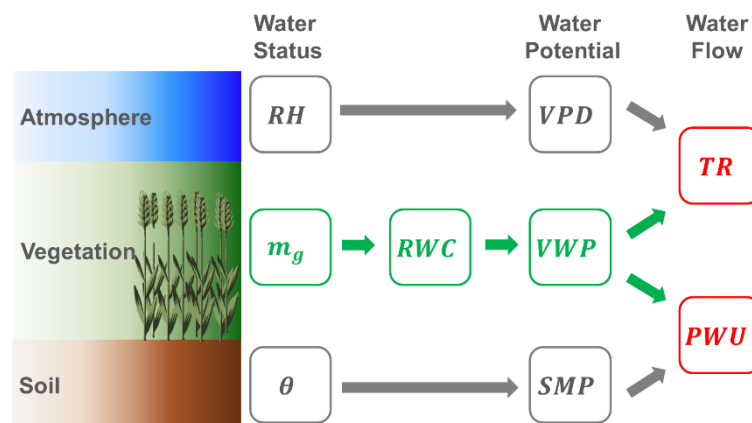
Figure 2: Processing workflow for estimation of soil, vegetation and atmosphere water potentials (SMP= soil matric potential, VWP = vegetation water potential, VPD = vapor pressure deficit) and water fluxes (PWU = plant water uptake, TR = transpiration rate) from storage variables (θ = soil moisture, m_g = vegetation water content (gravimetric), RH = relative air humidity); Green variables are derived from radiometer observations, while gray ones are calculated from in situ measurements; Red variables are derived jointly from radiometer and in situ observations.

3.1 Soil matric potential (*SMP*) from soil moisture (*θ*)

205   The fundamental force describing the overall state and movement of water within the soil is energy: kinetic or

potential (Hillel, 1980). The kinetic energy is assumed to be negligible in agricultural (wheat-covered) soils due to

the overall slow movement of soil water in fields with no to moderate slopes (Hillel, 1980; Shukla, 2014). The

potential energy, however, is important when describing the movement of water in soils and the water retention

forces against percolation towards ground water level. Hence, the rate of decrease in potential energy with distance

210   is actually the driving force which causes water to flow within soils (Hillel, 1980). The difference in energy states

between the soil water and pure free water (i.e. reference potential) is defined as the total soil water potential. In

unsaturated soils various forces, such as capillary or adsorption, act on soil water, which causes soil water potential

to be lower than that of pure water in reference conditions (known as suction tension).

    Due to the different forces influencing the soil water, the total soil water potential is mainly the sum of pressure,

215   gravitational and osmotic potentials (Hillel, 1980; Shukla, 2014). Since the pressure potential is defined as the

water potential resulting from capillary and adsorptive forces acting on the soil matrix, it is generally called the

SMP or matric suction (Hillel, 1980; Shukla, 2014); it can be expressed in energy per unit mass [*J/kg*], in energy

per unit volume (pressure: [*bar*] or [*Pa*]), or energy per unit weight (hydraulic head: [*cm*] or [*pF*]) (Hillel, 1980;

Shukla, 2014, Ward and Robinson, 2014).

220   The *SMP* is dependent on *θ* and vice versa. The relationship between both parameters is described by the soil

water retention curve. Water retention subsumes all mechanisms and processes related to changes of soil moisture

and its energy state (Gupta and Wang, 2006). The shape of the soil water retention curve is dependent upon various

soil characteristics (e.g., texture, and particularly clay fraction), as well as on the current and previous states of *θ*

(Hillel, 1980; Ward and Robinson, 2014).

225   When investigating plant growth, two common values of *SMP* are of major interest: the permanent wilting point

and the field capacity. The wilting point (around *SMP* of -1.5 [*MPa*]) is defined as the minimum soil water content

at which most crop plants can still extract water from the soil (Nobel, 2020, p. 542). The field capacity, reported

for instance at -0.01 [*MPa*] in Ward and Robinson (2014) or at -0.033 [*MPa*] in Gupta and Wang (2006),

corresponds to the amount of remaining water after a saturated soil drained under gravity for one to two days

230   following a precipitation event. Exact values for each soil are dependent on the individual soil characteristics. The

difference between field capacity and wilting point is regarded as available water that can be taken up by plants

(Ward and Robinson, 2014; Gupta and Wang, 2006). Besides tensiometer or thermocouple psychrometer, which

can directly measure SMP (Hillel, 1980; Gupta and Wang, 2006), several soil water retention models exist to estimate SMP from θ. The most widely used ones are from Brooks and Corey (1964), Campbell (1974), or Van Genuchten (1980). In this study we apply the Campbell model to estimate SMP from θ measurements:

$$SMP = \left(SMP_s * \left(\frac{\theta}{n} \right)^{-b} \right),$$ (1)

with SMP_s as matric potential at field capacity (saturated suction), n representing soil porosity, and b as empirically determined constant characterizing the pore-size distribution of the soil (Margulis, 2017; Campbell, 1974). The values for SMP_s and b for (1) are provided by Clapp and Hornberger (1978), where representative values for hydraulic parameters are presented for various soil textures. The values for the soil type silty loam at Selhausen are SMP_s = -0.786 [m], $n = \theta_s \cdot f_s$ (including soil moisture content at field capacity θ_s= 0.485 [-] from Clapp and Hornberger (1978) and silt fraction from soil surveys at the test site f_s=0.7 [-]) and b = 5.3 [-]. Values for θ originate from *in situ* relative permittivity measurements from 5 [cm] and 30 [cm] soil depth (cf. section 2).

3.2 Relative water content (*RWC*) and vegetation water potential (*VWP*) from vegetation moisture (m_g)

The m_g of the winter wheat field [kg/kg] was first estimated in Meyer et al. (2019) from ground-based L-band radiometer data, acquired between 9 am and 2 pm at 40° incidence angle. In this process, the VOD was retrieved via radiative transfer model inversion from the V-polarized brightness temperature measurements of ELBARA-II. Afterwards m_g was estimated from VOD by inversion of the forward model proposed by Schmugge & Jackson (1992) (Meyer et al., 2019; Ulaby and El-Rayes, 1987). Full details are provided in Meyer et al., 2019. m_g is a metric of kilogram water per kilogram wet biomass and can be converted into a change metric, called relative water content RWC [%] by putting boundaries on upmost (maximum $m_{g\,max}$) and lowest (minimum $m_{g\,min}$) m_g (Pearcy et al., 2012; Easmus et al., 2016; Smart and Bingham, 1974):

$$RWC = \frac{m_g - m_{g\,min}}{m_{g\,max} - m_{g\,min}} \cdot 100,$$ (2)

As these boundary conditions are found for this study along the measured growing season in 2017 within the winter wheat field, the RWC serves as a relative metric referring to the water dynamics of the recorded season (RWC_{Season}). Since m_g-estimates are obtained only once on a measuring day, it limits the chance of capturing the true minimum and maximum of the 2017 growing season. However, the $m_{g\,min}$ is found in the senescence phase

260   where the water content drops to a minimum (see low and constant level of VWC in Figure 1 for the senescence

phase). The detection of the maximum $m_{g_{max}}$ of the season is even more challenging due to the temporally sparse

measurements. Therefore, the maximum of the m_g-timeseries $m_{g_{max}}$ is used. Note that RWC_{Season} by definition

is not representative of water dynamics on shorter time scales than seasons, like on weekly or even diurnal scales

or for single phenological phases (Passioura, 1982).

265   For the next step, Zweifel et al. (2000; 2001) described a semi-empirical model linking the RWC [%] to its VWP

[MPa]:

$$VWP = \frac{VWP_{min}}{e^{\frac{-k_1 + RWC}{k_2}} + 1},$$
(3)

where k_1 and k_2 are empirical parameters representing the inflection point of the function, and the rate of change

between RWC and VWP, respectively. VWP_{min} [MPa] is the minimum of VWP assumed for the relationship.

270   All three parameters are plant type specific and need plant-specific adaption, since the parameterization of Zweifel

et al. (2000; 2001) was done for trees. In this study we adapted the parameterization for winter wheat with VWP_{min}

of -2.5 [MPa] (Frank et al., 1973; Gupta et al., 1989; Kameli and Lösel, 1993; Rascio et al., 1994, Siddique et al.,

2000). Figure 3 illustrates the RWC-VWP relationship for slow (k_1=55; k_2=10), intermediate (k_1=68; k_2=7.5)

and rapid (k_1=81; k_2=5) change dynamics according to literature studies (Turner and Long, 1980; Turner, 1988;

275   Zweifel et al., 2001; Pearcy et al., 2012; Konings et al., 2019). The sigmoidal dynamics in Figure 3 should cover

the potential variation of dynamics for wheat, as understood from literature. It is in no means exhaustive or fully

precise.
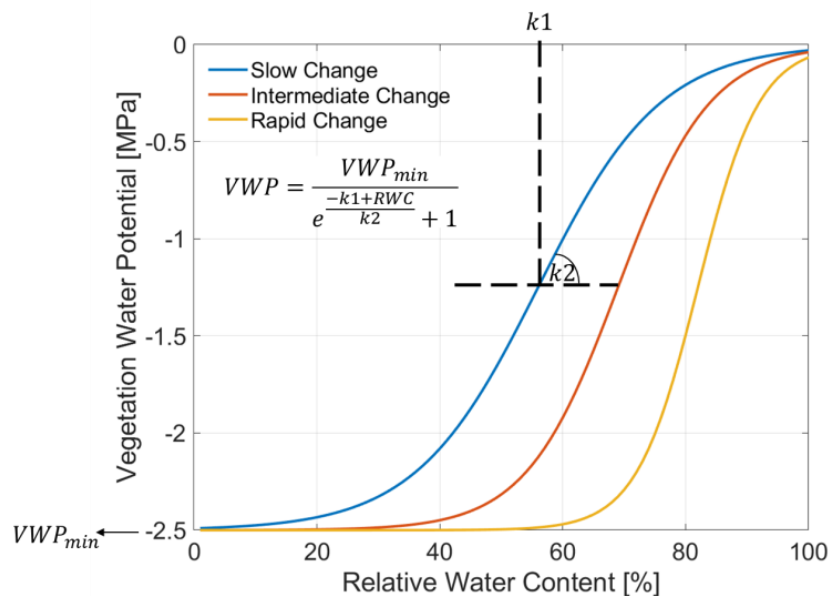
Figure 3: Modelled relation between relative water content (*RWC*) [%] and vegetation water potential (*VWP*) [*MPa*] adapted for winter wheat and assuming different rates from slow (blue color) to intermediate (red color) until rapid (orange color) change. The inset equation, adopted from Zweifel and Häsler (2000) and Zweifel et al. (2001), integrates a minimum *VWP* (VWP_{min}) and specifies an inflection point (k_1) and a rate (k_2) of the change dynamic between *RWC* and *VWP*. k_1 and k_2 are also indicated schematically with dashed black lines.

3.3 Atmosphere water potential (vapor pressure deficit - *VPD*) from relative humidity (*RH*) and air temperature (T_{Air})

In unsaturated air conditions the atmosphere shows a deficit of water vapor indicating the water potential of the atmosphere. Atmospheric vapor pressure deficit (*VPD*) is defined as the difference between the actual water vapor pressure and the saturation water vapor pressure at a particular temperature. It can be calculated as follows (Reichardt and Timm, 2014; Castellvi et al., 1996):

$$VPD = P_{sa}(1 - RH), \qquad (4)$$

Including the relative humidity of the air *RH* [-] and saturation water vapor pressure of the air $P_{sa} = 0.61094 \cdot \exp(17.625 \cdot T_{Air}/(T_{Air} + 243.04))$ [*kPa*], where T_{Air} represents the air temperature [°*C*] (Alduchov and Eskridge, 1996). In this study *RH* and T_{Air} are measured at 2 [*m*] height above ground at the on-site meteorological station. Time series of *VPD* and its input variables (*RH*, T_{Air}) for the period of study are presented in Figure 4.
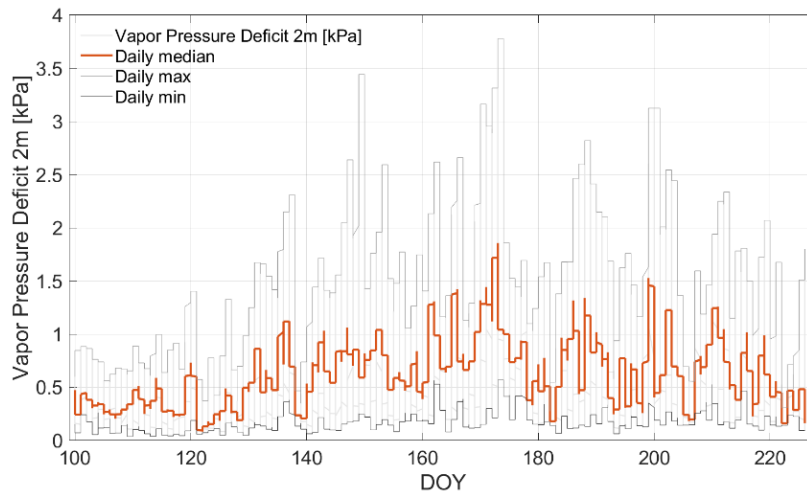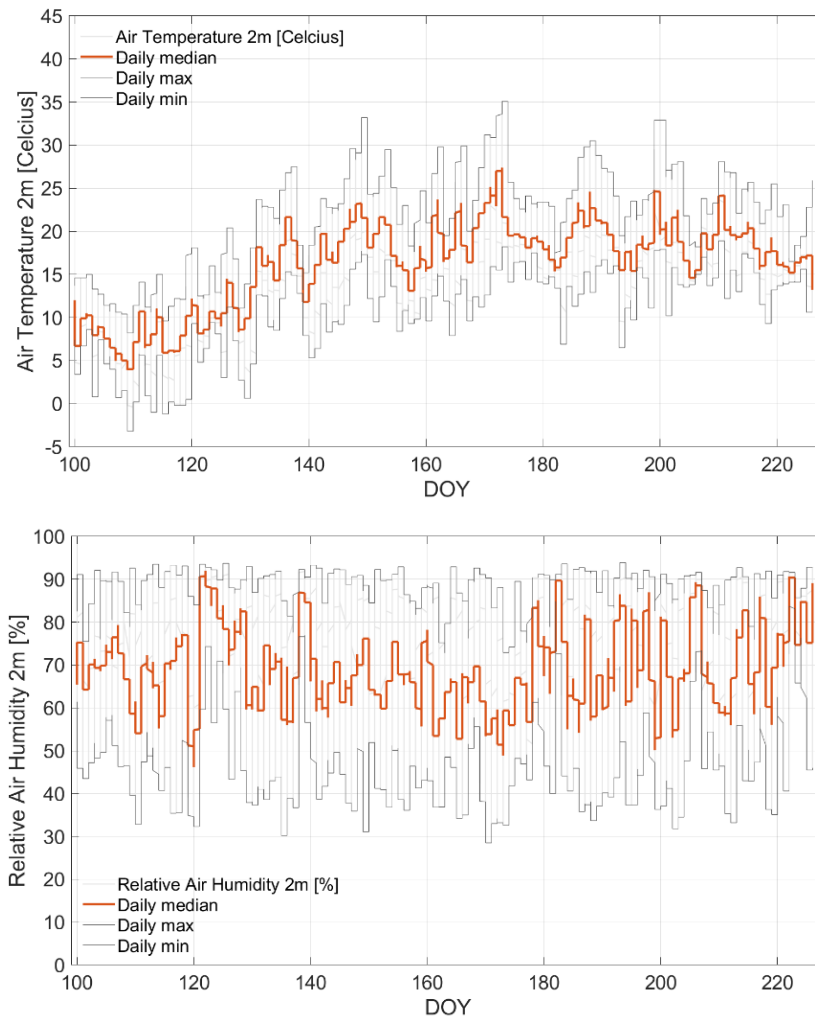
300

Figure 4: Calculated vapor pressure deficit (VPD [kPa]) at 2 [m] height (top plot) from measurements of air temperature ([T [$°K$]) (middle plot) and relative humidity (RH [%]) (bottom plot) using Equation (4) in the growing period of 2017 along days of year (DOY) in 2017 at the winter wheat field in Selhausen, Germany. Colored and gray curves indicate daily median, minimum and maximum of measurements and estimates.

305

3.4 Water uptake (PWU) from soil into the wheat plants

The water uptake process follows from hydraulic potential gradients and flow resistances in the SPAS. The principle of potential difference by flow resistance is motivated from the field of electricity by Ohm's law. Van den Honert (1948) was one of the first who showed this connecting concept (Cowan, 1965, Monteith and Unsworth, 2013; Nobel, 2020).

310

The PWU [mm/s] from the soil into the winter wheat plant can be defined as the potential difference (converted to [mm]) between the soil (SMP) and the vegetation (VWP) divided by the resistance (e.g. in the rhizosphere, roots and xylem along SPAS (Van den Honert, 1948; Wallace, 1978; Wallace and Biscoe, 1983)):

$$PWU = \frac{SMP - VWP}{R_{RX} + R_S},\tag{5}$$

315

where R_{RX} $[s]$ is the resistance to water flow in roots and xylem of the wheat plants (Lynn & Carson, 1990) and R_S $[s]$ is the resistance to water uptake from the soil into the wheat roots. Since R_S and R_{RX} cannot be measured in situ at field scale along the growing season (Wallace, 1978; Wallace and Biscoe, 1983; Ruggiero et al., 2007), all resistances in this study are effective values with no claim on absolute accuracy.

320 We adopted the approach of Feddes and Rijtema (1972) estimating the R_S from soil hydraulic conductivity $[m/s]$, based on the Campbell model (Campbell, 1974; Choudhury and Idso, 1985; Lynn and Carlson, 1990; Dingman, 2015; Meyer et al., 2018). We used soil moisture $[m^3/m^3]$ (converted from soil permittivity) and soil parameters for silty loam from Clapp and Hornberger (1978) and Steenpass et al. (2010), and a rooting depth of one meter according to literature (Fan et al., 2016). Figure 5 shows estimates of soil resistance $[s]$ from Feddes and Rijtema (1972) based

325 on soil hydraulic conductivity $[m/s]$ at 5 $[cm]$ and 30 $[cm]$ soil depth.
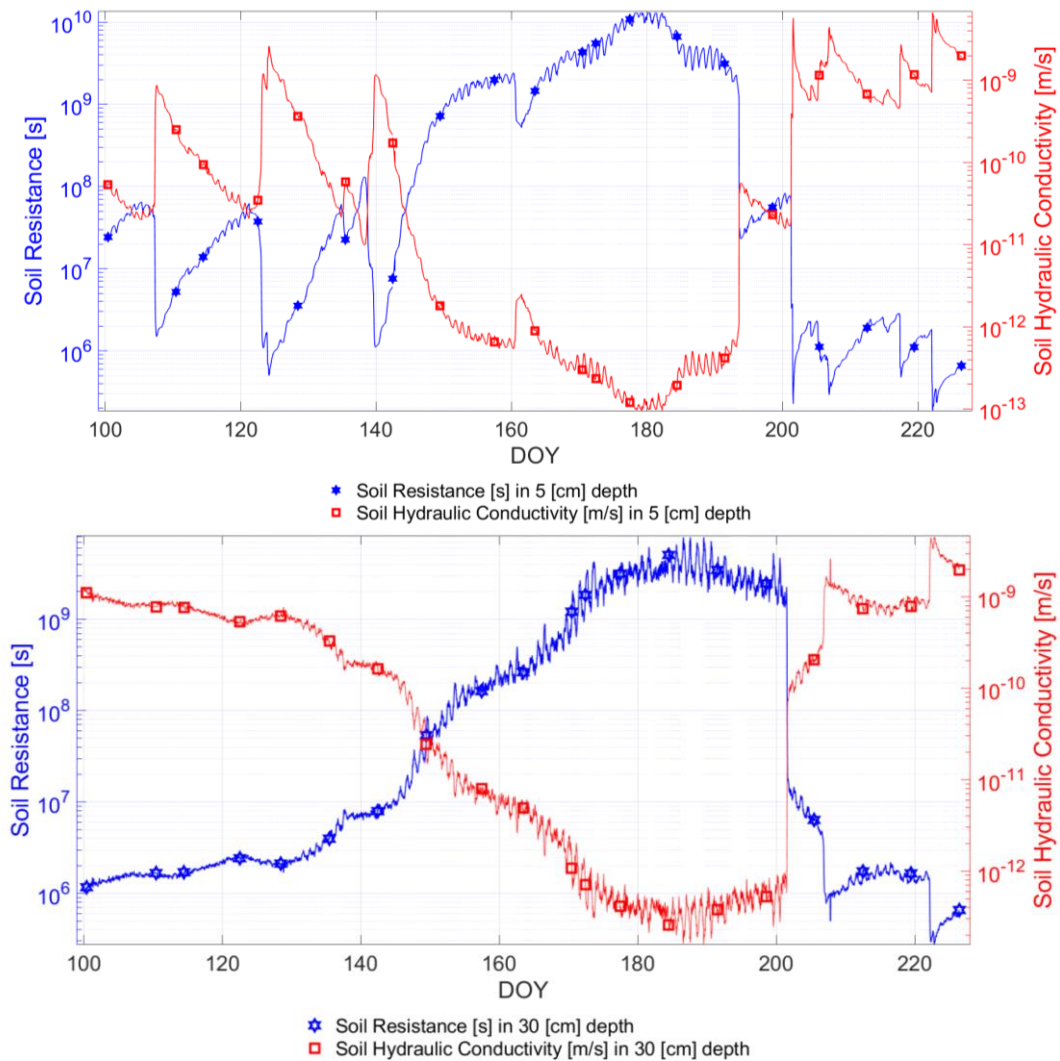
Figure 5: Comparison of the soil permittivity-derived and Campbell (1974) model-based soil hydraulic conductivity [m/s] and the calculated soil resistance R_S [s] from the model of Feddes and Rijtema (1972) implemented according to Choudhury and Idso (1985): at 5 [cm] (top) and 30 [cm] (bottom) soil depth; symbols indicate radiometer observation dates along days of year (DOY).

335

For the root-xylem resistance R_{RX} we deduced a LAI-based linear model from an approach combining in situ measurements with boundary layer modelling, detailed in Lynn and Carlson (1990, Fig. 16):

$$R_{RX} = (-LAI \cdot 0.007 + 0.05) * C_U, \tag{6}$$

340

where LAI [m^2/m^2] was measured in situ (cf. Fig. 1) and $C_U = 0.4 \cdot 10^{10}$ represents the unit conversion from [$bar\,(W/m^2)^{-1}$] to [s]. The coefficients in (6) are empirically derived from the study of Lynn and Carlson (1990) on corn. It is to note that the relationship for winter wheat may be different than for corn. However, due to its

345 simplicity (linear correlation with LAI) it allows dynamizing the root-xylem resistance along the growing season,

while keeping the amount of needed input variables constant. Figure 6 shows R_{RX} along the growing period and its linear relation to LAI.
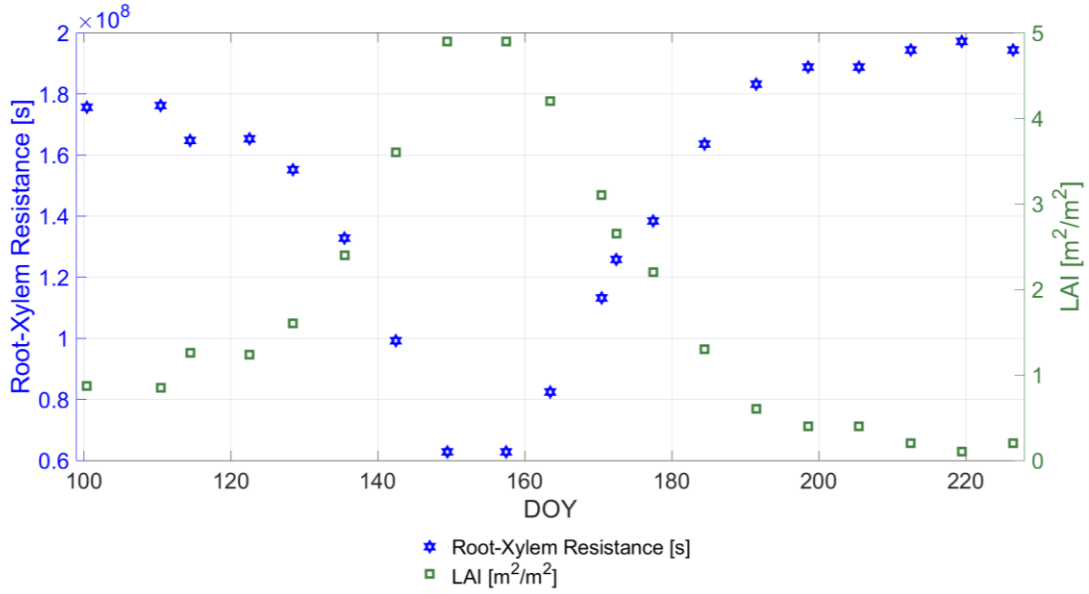
Figure 6: Comparison of the in situ-measured leaf are index LAI $[m^2/m^2]$ and the calculated root-xylem resistance R_{RX} $[s]$ deduced from Lynn & Carlson (1990) along days of year (DOY).

3.5 Transpiration (TR) from wheat plants into atmosphere

The wheat transpiration rate TR $[mm/s]$ from the wheat plants into the surface-proximate atmosphere is expressed as the potential difference between the vegetation (VWP) and the atmosphere (VPD) (at 2 $[m]$ height above ground) divided by the resistances against transpiration. These latter are the resistance of the upper (adaxial) and lower (abaxial) side of the leaves and their respective stomata to water vapor outgassing and the resistance of the surrounding atmosphere (Reichardt and Timm, 2014, p.277ff; Pearcy et al., 2012, p175ff; Nobel, 2020, p.415ff):

$$TR = \frac{VPD - VWP}{R_A + 2R_C + 2R_{ST}}, \tag{7}$$

where R_A $[s/m]$ is the aerodynamic resistance of the proximate atmosphere to the absorption of the vaporized moisture (Allen et al., 1998; Monteith, 1965; Chouhury and Idso, 1985). R_C $[s/m]$ is the cuticular resistance of the leaf surface for direct transpiration through epidermis (fixed to $R_C = 4 \cdot 10^3$ $[s/m]$) (Monteith and Unsworth, 2013; Nobel, 2020, p.415). R_C is of minor influence in this study due to non-drought conditions (Duursma et al., 2019). It is included for simplicity as an additive resistance component in (7) (Nobel, 2020, p.427ff). R_{ST} $[s/m]$ is the resistance of the wheat canopy stomata to transpiration (Gallardo et al., 1996). Damour et al. (2010) provide a comprehensive overview of stomatal resistance models. Choudhury and Idso (1985) proposed an empirical model

for canopy stomatal resistance of field-grown wheat stomata. It is adopted in the following to provide estimates of time-varying stomatal resistance $[MPa\,s/m]$ values for the winter wheat field (Choudhury and Idso, 1985), where density of liquid water (997 $[kg/m^3]$) and latent heat of water vaporization ($2.2564 \cdot 10^6$ $[J/kg]$) are used to convert

370   units from $[s/m]$ to $[MPa\,s/m]$ to match the calculus in (7) (Monteith & Unsworth, 2013). On-site measurements of solar net radiation $[W/m^2]$ (cf. Fig. 1) and VWP were used as inputs to the model. The net radiation as well as the stomatal resistance R_{ST}-values are displayed in Figure 7 and compared to values reported in Nobel (2020, p. 421). Details of the implementation are provided in Choudhury and Idso (1985).

The aerodynamic resistance R_A, shown in Figure 8, is a function of the wind speed (measured at 2 $[m]$ height) and

375   the vegetation height (cf. Fig. 1). The R_A-calculus was adopted from Monteith,1963. This definition was also adopted by Allen et al. (1998) and Choudhury and Idso (1985).

Both resistance values (R_{ST}, R_A) are used together with R_C in (7) to calculate time-dynamic transpiration rates TR.
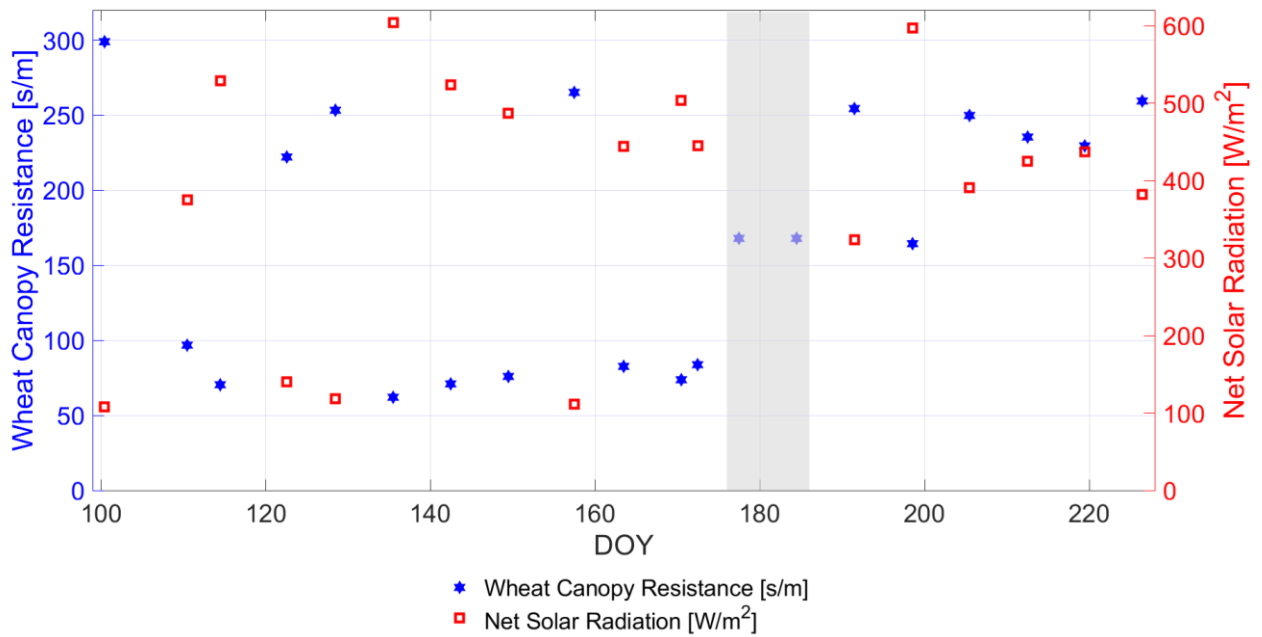
380   **Figure 7: Comparison of the in situ measured net solar radiation $[W/m^2]$ and the calculated stomata resistance R_{ST} $[s/m]$ of the winter wheat canopy from the model of Choudhury and Idso (1985) under incorporation of VWP-observations (cf. Figure 1) along days of year (DOY); The gray area indicates two dates where no net solar radiation measurement were available and the resistance values for the canopy are set to fixed values of 168 $[s/m]$.**
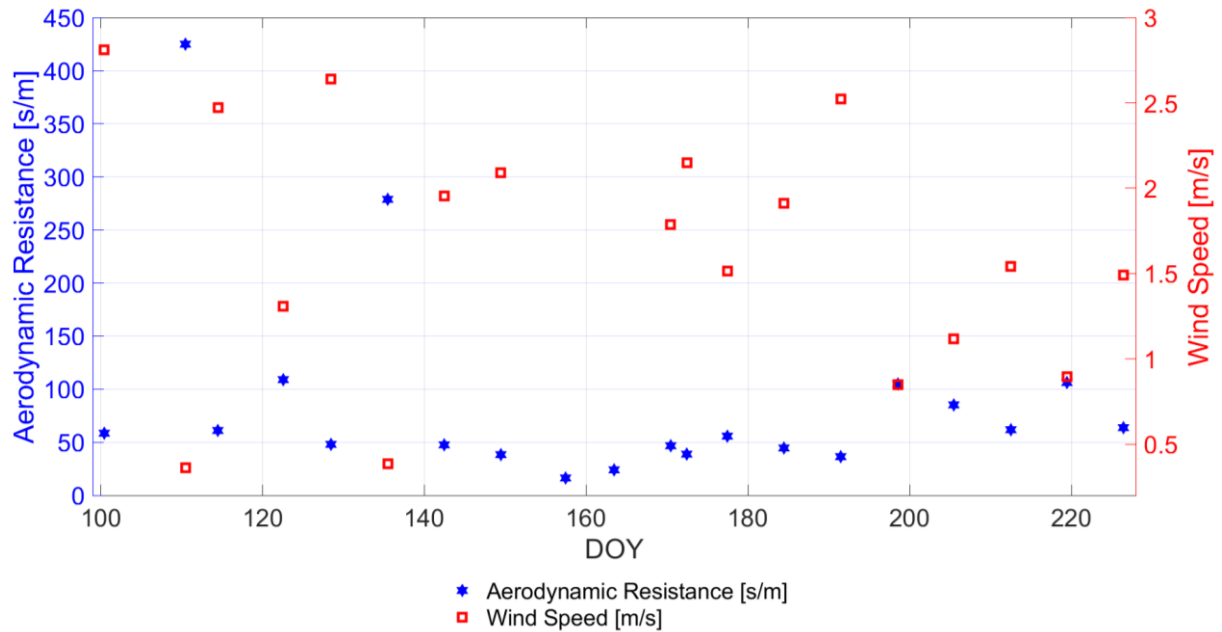
385

Figure 8: Comparison of the in situ measured wind speed $[m/s]$ and the calculated aerodynamic resistance R_A $[s / m]$ of the winter wheat canopy from the model of Monteith (1963) (adopted in Choudhury and Idso (1985)) under incorporation of vegetation height observations (cf. Figure 1) along days of year (DOY).

390

Since R_A, R_C and R_{ST} are effective values (Wallace, 1978; Wallace and Biscoe, 1983) and not directly measurable in situ for an entire wheat field (Selhausen test site) along the full growth period (April to August 2017) (Ruggiero et al., 2007; Blizzard and Boyer, 1980), they were retrieved in a model-based way as introduced above.

Table 2 provides a summary on the non-measured variables for estimation of plant water dynamics that were

395 obtained from parameterizations and models in this study.

Table 2: Summary of parameterizations and models for the non-directly measured variables in the estimation of plant water dynamics of winter wheat.

Variable	Parameterization	Model / Reference
Soil		
Soil matric potential (SMP) [MPa]	Soil moisture, soil porosity n, soil texture (sand, silt & clay fractions) & pore size distribution b	Campbell, 1974; Clapp and Hornberger, 1978
Vegetation		
Relative water content (RWC) [%]	Gravimetric water content of winter wheat m_g	Pearcy et al., 2012; Smart and Bingham, 1974
Vegetation water potential (VWP) [MPa]	RWC & empirical calibration parameters (k_1, k_2)	Zweifel and Häsler, 2000; Zweifel et al., 2001
Plant water uptake (PWU) [mm/s]	VWP, R_S, R_{RX} & SMP	Monteith & Unsworth, 2013; Wallace, 1978; Van den Honert, 1948
Soil resistance (R_S) [s/m]	Soil moisture, soil texture & rooting depth	Feddes and Rijtema, 1972; Campbell, 1974; Clapp and Hornberger, 1978
Root-xylem resistance (R_{RX}) [s/m]	LAI	Lynn & Carlson, 1990
Transpiration rate (TR) [mm/s]	VWP, R_C, R_{ST}, R_A, & VPD	Reichardt and Timm, 2014, p.277ff; Pearcy et al., 2012, p.175ff; Monteith & Unsworth, 2013, p.191
Stomatal resistance (R_{ST}) [s/m]	Solar net radiation & VWP	Choudhury and Idso, 1985
Aerodynamic resistance (R_A) [s/m]	Wind speed & vegetation height	Allen et al., 1998; Choudhury & Idso, 1985, Monteith, 1965
Atmosphere		
Vapor pressure deficit (VPD) [kPa]	Relative air humidity & P_{sa}	Castellvi et al., 1996;
Saturation water vapor pressure (P_{sa}) [kPa]	Air temperature	Alduchov and Eskridge, 1996

400

4 Results

The results are presented following the SPAS from soil to atmosphere. The following sections discuss the water status in the soil and wheat plants, moving on to, the water dynamics from the soil via wheat plants into the surface-proximate atmosphere.

4.1 Water status in the soil

In Figure 9, the estimated SMPs at 5 [cm] and 30 [cm] soil depth are shown together with the soil permittivity of the top soil (5 [cm] below surface) and in the root zone (30 [cm] below surface) as well as the daily sum of precipitation.

For top soil, highest permittivity values are reached after the early senescence with ~15.5 [-], corresponding to a soil moisture value of ~28.4 [$vol.\%$]. From DOY 160 to DOY 190 the soil permittivity stays at a low level of ~9 [-] (~16.8 [$vol.\%$]), since during that period almost no precipitation occurred. The high correlation between the SMP and soil permittivity curves at 5 [cm] as well as at 30 [cm] soil depth is a result of the fact that soil permittivity is one of the main input parameters within the Campbell model to determine SMP, and, in addition, due to the water retention characteristics between θ and SMP (cf. section 3). After every rain event when soil permittivity increases, the SMP also increases towards less negative values. This is more pronounced for the top soil layer than for the deeper one.

As the empirically fitted parameter b in (1) was set to 5.3, the obtained soil water retention curve is non-linear. This effect is visible during the dry period between DOYs 140 to 190, where the SMP constantly decreases to more and more negative values until DOY 180 and then increases towards less negative values again. While the soil permittivity decreases, the SMP takes on more negative values. For SMP at 30 [cm] soil depth, the drying period starts at DOY 150, which is slightly delayed in time compared to the start of the drying period of SMP at 5 [cm] soil depth, as indicated in Fig. 9. The drying period affects the deeper soil layers longer (until DOY 200). Furthermore, at around DOY 185 the maximum suction tension with -0.15 [MPa] at around DOY 185 is lower (by 0.05 [MPa]) for soil in the root zone than for SMP in the top soil.

If SMP at -0.033 [MPa] is considered as field capacity, the estimated results always indicate enough available water for plants to be extracted from the soil across the entire period of investigation. However, if one considers the SMP at -0.01 [MPa] as field capacity, the winter wheat may have less available water some times during the stem elongation and after the early senescence phases. However rooting depth was not measured along the growing season of 2017, even though it would provide information about the respective water reservoirs assessible for the wheat plants during the different phenological phases. During the period between DOY 178 and DOY 182 the results for SMP at 5 [cm] depth show the highest suction tensions with values down to -0.2 [MPa], whereas the permanent wilting point is around -1.5 [MPa]. This indicates a drier period for the wheat plants, although water from the soil was available for the plants at any time during the growing season (cf. section 3).
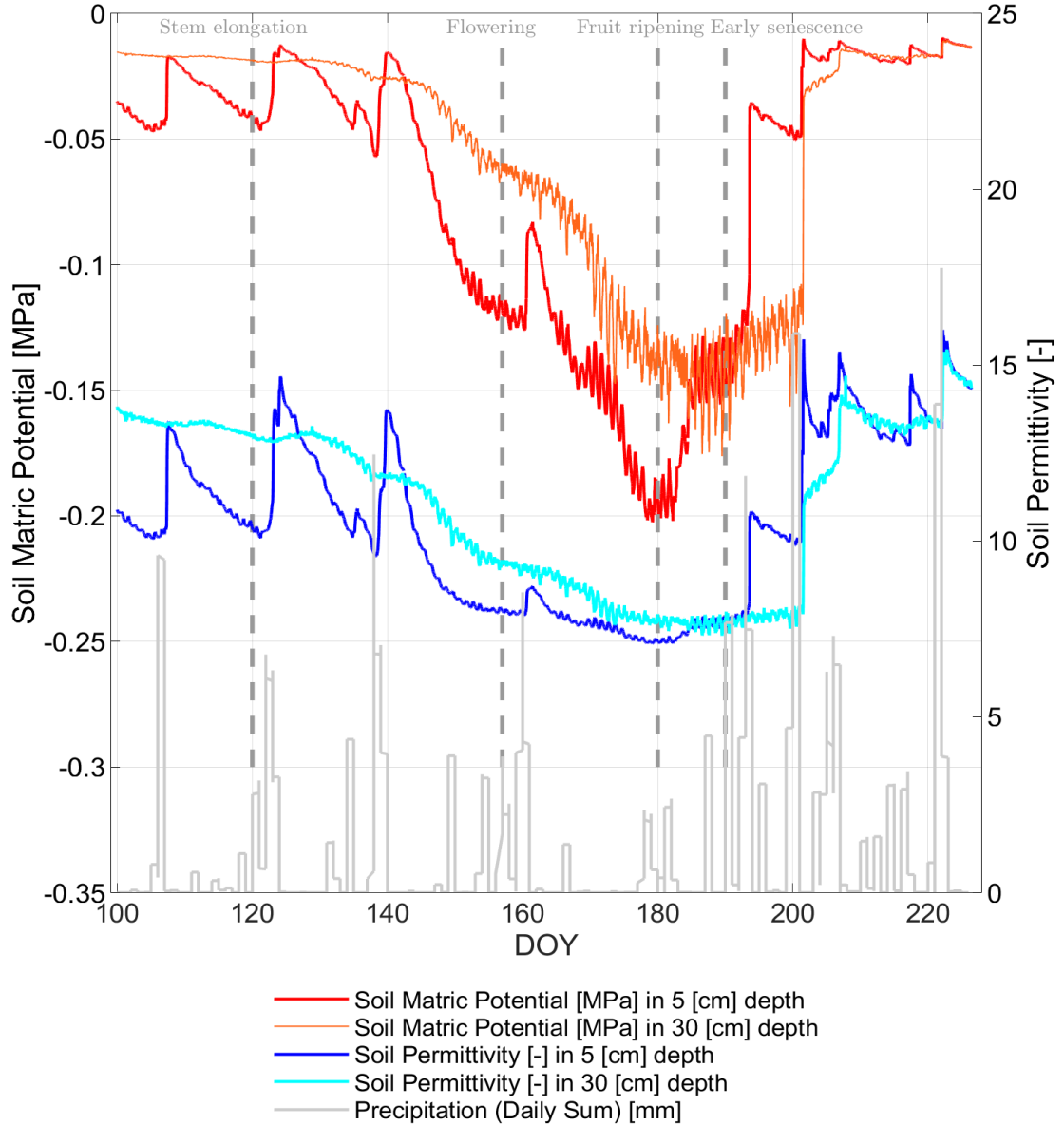
Figure 9: Comparison of the temporal evolution of soil matric potential (*SMP*) [*MPa*], calculated after Campbell (1974) & Clapp and Hornberger (1978) in 5 [*cm*] (red curve) and 30 [*cm*] (orange curve) soil depth from in situ measured soil permittivity [-] in 5 [*cm*] (blue curve) and 30 [*cm*] (cyan curve) throughout growing season of 2017 in days of year (DOY). Gray bars indicate the daily sum of precipitation [*mm*] at the winter wheat field in Selhausen, Germany.

4.2. Water status in wheat plants

In order to understand the vegetation status along growing season, m_g [*kg/kg*] of the winter wheat is calculated according to Meyer et al. (2019) from radiometer observations and presented in Figure 10. We assumed vertical stalks as mainly affecting plant component of winter wheat for L-band emission and within radiometer-based m_g-calculus for subsequent analysis in this study. Figure 10 indicates the in situ measurements (gray crosses), described in section 2, and the radiometer-based estimates (blue circles) of m_g over the wheat growing period (senescence from DOY 191). The overall dry down of the winter wheat along growing season accompanied by the ripening of

the plants until senescence is tracked by in situ measurements as well as by the radiometer-based m_g-estimates, despite both are statistically independent entities.

From Figure 10, it becomes apparent that the estimates yield a higher m_g-level in comparison with the in situ measurements in the senescence phase (cf. Fig. 10, DOY 200-226), which can be explained by assuming in the retrieval of Meyer et al. (2019) that the vegetation volume fraction stays constant along the growing season. This is a strong, but unavoidable assumption as long as auxiliary information on vegetation volume fraction, as seen by a microwave L-band radiometer, is not at hand. At the moment, no measurements for the vegetation volume fraction from L-band radiometers exist according to the authors' knowledge. More details on the retrieval of the gravimetric water content shown in Figure 10 are provided in Meyer et al. (2019).
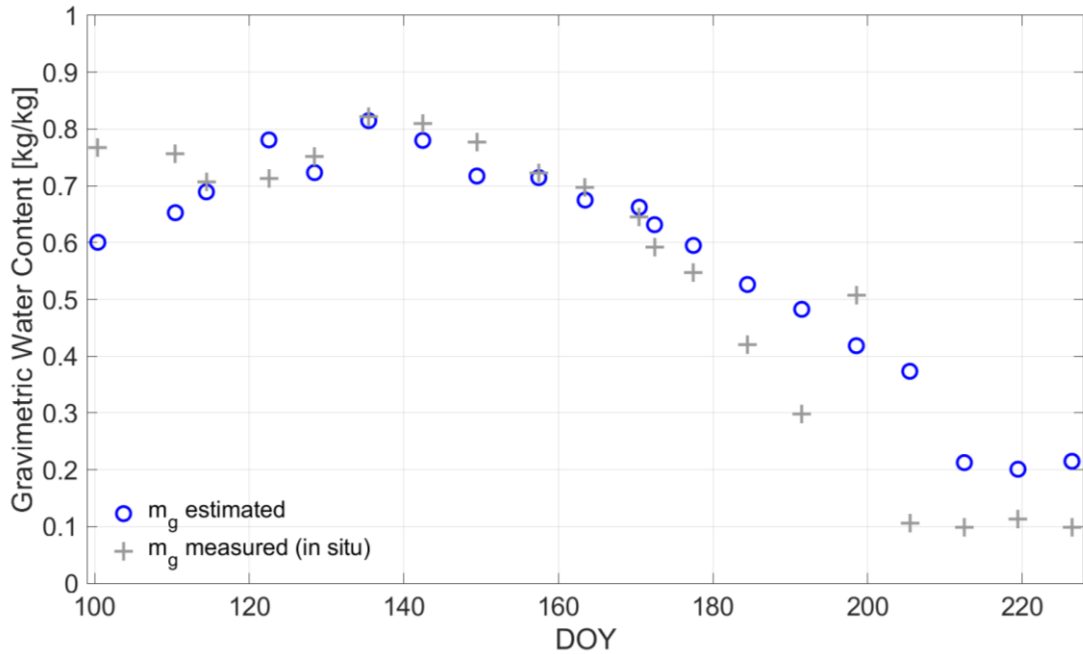
Figure 10: Measured (gray crosses) and radiometer-derived (blue circles) gravimetric vegetation water content (m_g) [kg/kg] of winter wheat along days of year (DOY) in the growing season of 2017 at the field laboratory in Selhausen, Germany (Meyer et al., 2019).

In Figure 11, the RWC_{Season} is shown for the entire growing period after calculus from (2) based on m_g. A contrasting way of calculating RWC_{Season} [%] from radiometer-based methods is reported in Rao et al. (2019), but adopted by using the extremes of the VOD along growing season:

$$RWC_{Season,VOD} = \frac{VOD - VOD_{min}}{VOD_{max} - VOD_{min}} \cdot 100, \tag{8}$$

where VOD_{min} and VOD_{max} are the minimum and maximum of VOD within the recorded time series. By calculating RWC_{Season} in this way, it is assumed that VOD is a direct indicator for m_g in wheat and does not depend on biomass or vegetation structure. But, as can be seen from the course of $RWC_{Season,VOD}$ along growing period (cf. Fig. 11), the water content is low for DOY 100 (tillering), since RWC-values are below 10 [-]. Afterwards, they increase until DOY 157 (onset of flowering with peak of vegetation height at DOY 149) to the level of RWC_{Season}, calculated from (2). In this phase from tillering to flowering, also the main biomass and plant structure developments of the wheat plants took place (cf. Fig. 1) and are also included in the VOD-signal (Momen et al., 2017). This indicates one shortcoming of assessing the water content directly on basis of VOD, like in (8) (Fink et al., 2018; Meyer et al., 2019). However, in periods of constant biomass, meaning times where only the water content in the plants would change, RWC_{Season} could be directly estimated from VOD (Rao et al., 2019; Holtzman et al., 2020; Xu et al., 2021).
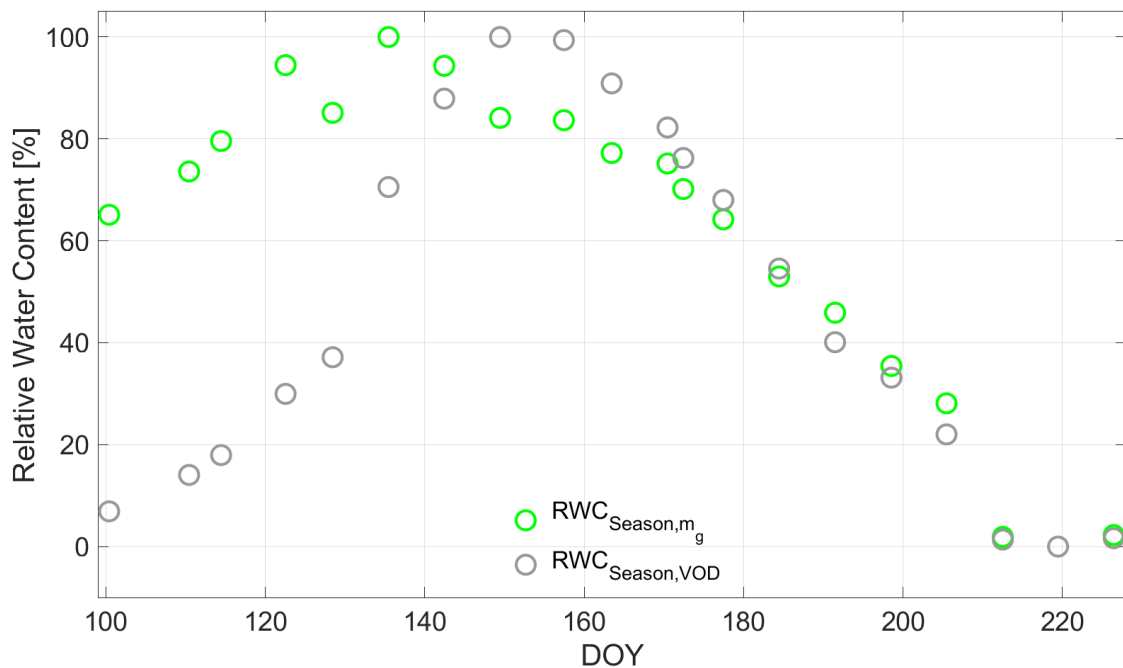
Figure 11: Seasonal relative water content (RWC_{Season}) [%] calculated in (2) with radiometer-derived m_g (green circles) along growing season of 2017 in days of year (DOY) at the winter wheat field in Selhausen, Germany. The gray circles indicate RWC_{Season} calculated directly with the radiometer-derived vegetation optical depth (VOD) according to (9).

From RWC_{Season}, the VWP of the winter wheat can be retrieved using (3) and assuming different change rates of VWP according to RWC_{Season}-dynamics (cf. Fig. 3). Figure 12 shows in green color the intermediate change rate and in a gray area between dashed curves the behavior of the VWP according to the different assumed change rates (blue color: slow change rate & red color: rapid change rate).

Hence, the influence of k_1 and k_2 in (3) is evident. The three different change rates (slow, intermediate and rapid) represent the possible spread of occurring $RWC\text{-}VWP$ relationships for winter wheat and provide a potentially occurring VWP-value range resulting from the different change rate assumptions.

The common trends of the VWP-value range might be interpreted as guided by the precipitation inputs along the growing season (cf. Fig. 9): SMP in the top soil (0-5 [cm]) and in the deeper soil layers (30 [cm]). The SMP increases to less negative values with each infiltrating precipitation impulse.

Then, SMP gradually decreases in periods of dry downs (between the rain events, e.g. DOY 165 to DOY 175). VWP is not following SMP at any depth from DOY 100 to DOY 140. This might be partly due to the distinct phenological changes (stem elongation) or the lower temperature regime, since mean daily temperatures can be seen to slowly increase from around 10 [$°C$] to about 20 [$°C$] in these 40 days (cf. Fig. 4). In addition, the vegetation water potential matches the SMP-values close to zero in this period (cf. Fig. 12). This indicates a sufficient water supply (close to or at field capacity) of the wheat plants with sufficient canopy hydration.
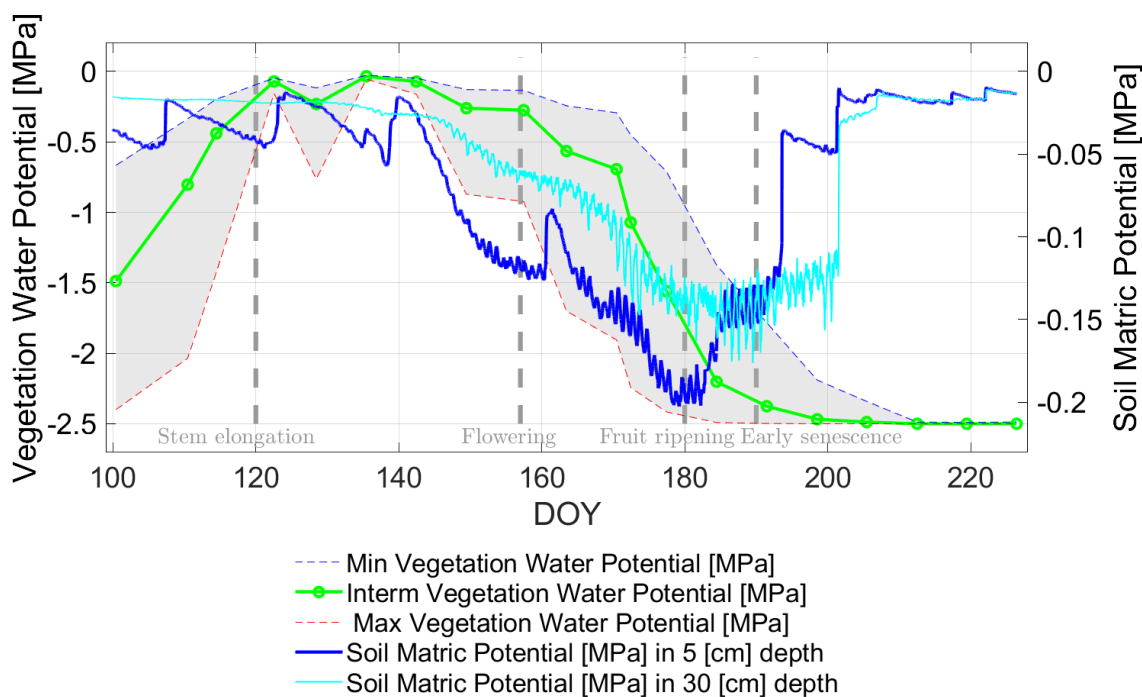
Figure 12: Comparison of in situ-based soil matric (both blueish curves) and radiometer-based vegetation water (green solid and small dashed curves) potentials (SMP [MPa] & VWP [MPa]) in the growing period of 2017 along days of year (DOY) at the winter wheat field. The gray-shaded area indicates the potential variability of the estimated VWP depending on applied relationship in (3) (cf. Fig. 3). Vertical dashed lines indicate major phenological phases of the winter wheat.

A distinct decrease in VWP to more negative values occurs between DOY 140 and DOY 180. In line with results from Choudhury and Idso (1985), this decrease to strongly negative values is concurrent with a period of low rainfall

and high evapotranspiration due to higher air temperature with a daily mean of around 20 $[°C]$ (cf. Fig. 4) and the maturation of the wheat in fruit development stage towards full biomass stage at DOY 191 (cf. also Tab. 1). Moreover, the different sampling rates for SMPs and VWP should be kept in mind, as SMPs and VWP originate from different sources ($SMPs$: in situ soil moisture measurements, VWP: L-band radiometer observations). However, the trend of both potentials (soil & vegetation) for the period of fully developed wheat canopy from DOY 140, with peak LAI at DOY 149 (cf. Fig. 4), to DOY 180 is apparently consistent with the in situ conditions of a diminishing water availability in soil and subsequently for the wheat plants.

Due to the onset of senescence in the wheat stand (latest DOY 200), the water supply of the drying plants degrades in importance, as the fruit (grains) ripen, meaning decreasing its content of liquid in the grains (Steduto et al.,2012; Sarto et al., 2017). Hence, water availability is not the limiting factor anymore and the concurrency of SMP and VWP trends vanishes completely. $SMPs$ at both depths increase to less negative values by a series of irregular rain events starting from DOY 180. VWP reaches the minimum of -2.5 $[MPa]$ (cf. Fig. 12) at around DOY 200. This indicates that water loss in the plant due to senescence processes (strong increase of R_{RX}) reached a stage where water content (m_g) falls to a minimum. Subsequently, VWP reaches its pre-defined minimum value (VWP_{min} = - 2.5 $[MPa]$), which was set for the semi-empirical relationship between water content and water potential (cf. (3) and Fig. 3).

4.3. Seasonal water dynamics along the SPAS

Previous results (Figs. 10-12) presented the water filling status and the water potential in soil and wheat vegetation. The results are now taken one step further by using the differences of the potentials (between atmosphere & vegetation as well as between vegetation & soil) together with soil, plant and atmosphere resistance estimates to assess water fluxes from soil to atmosphere: PWU and TR.

In Figure 13 the PWU $[mm/s]$ (bluish curves) is depicted as time-variable uptake (depending on soil and root-xylem resistances used in (5)) together with its radiometer-based input parameter VWP (green curve). The other input parameter in equation (5) is SMP which is illustrated in Figure 10 for both soil depths.

The blue PWU-curves in Figure 13 show an overall decline of water uptake until DOY 122. This results from a sufficient supply by precipitation water (SMP < -0.05 $[MPa]$) under low evaporative conditions (daily mean of VPD < 0.5 $[kPa]$ & of air temperature around 10 $[°C]$) and wheat plants in tillering and early stem elongation phase,

but without major biomass development (DOY 122: LAI = 1.24 [-], plant height = 0.25 [m] & above ground biomass = 0.24 [kg/m^2]; all values from Fig. 1 & Tab. 1).
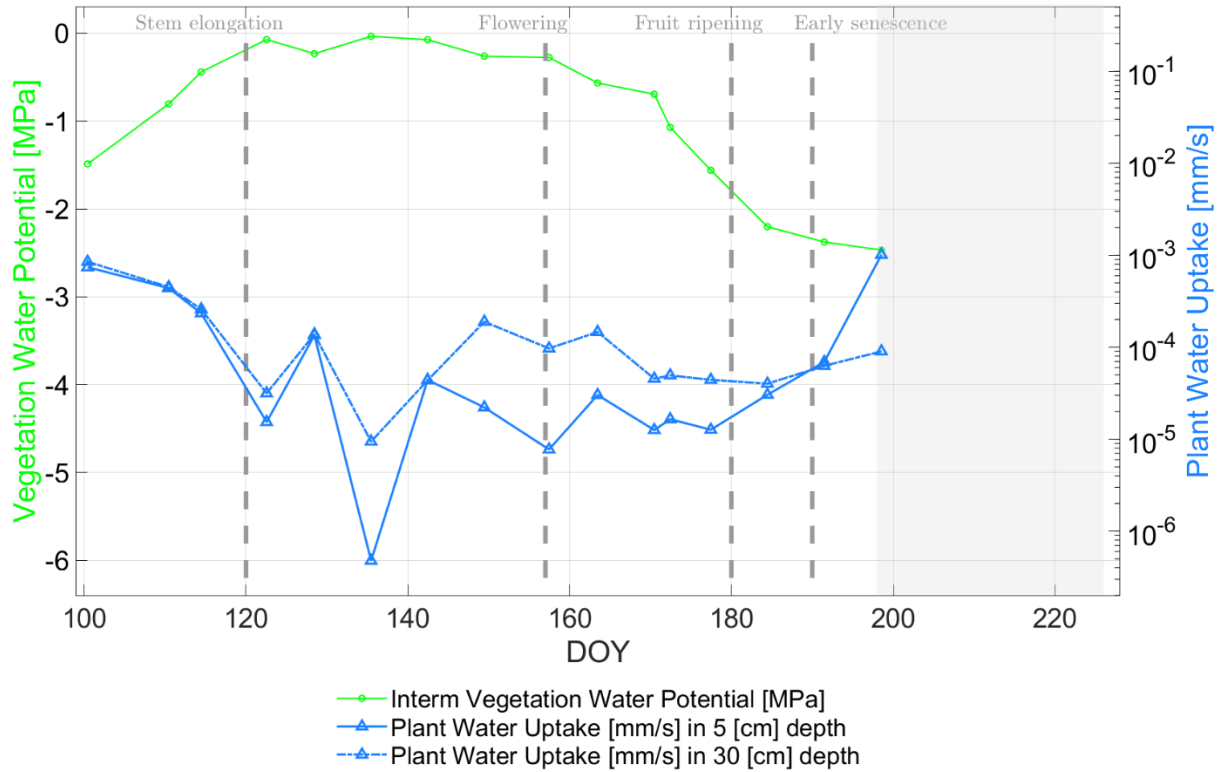
Figure 13: Comparison of radiometer-based plant water uptake PWU [mm/s] (blueish-colored curves with variable soil resistance at 5 [cm] and 30 [cm] soil depth) and vegetation water (green solid curve) potential VWP [MPa] along the growing season of 2017 for days of year (DOY) at the winter wheat field in Selhausen, Germany. The gray-masked area indicates the senescence phase where the water uptake estimates are not valid anymore due to simplifying assumptions in calculus of the root-xylem resistance. Vertical dashed lines indicate major phenological phases of the winter wheat.

540

From DOY 122 to DOY 142 (stem elongation phase) the biomass level increased slightly, but due to the wheat stalk development, the vegetation height and LAI changed significantly from 0.25 [m] to 0.56 [m] and 1.24 [-] to 3.6 [-], respectively (cf. Fig. 1). Moreover, the soil hydraulic conductivity and the respective soil flow resistance R_S (cf. Fig. 5) showed a steady decrease in water flow conditions at 30 [cm] depth and a fluctuating behavior due to rain impulses at 5 [cm] depth. Hence, the PWU-curves (blueish lines in Fig. 13) show the same trends for 30 [cm] and 5 [cm] depth having a lower level of PWU at shallower soil depth resulting from smaller soil hydraulic conductivity values (cf. Fig. 5). The lowest PWU-values in the range of $10^{-6} - 10^{-5}$ [mm/s] are supported by analysis of Cai et al. 2018, working at the same test site (Selhausen) and the same crop type (winter wheat), but already in 2016. The root-xylem resistance R_{RX} in Figure 6 indicates a steady decrease until DOY 142, clearly following its driving parameter LAI. The assumption behind is an increase in roots and xylem vessels concurrent to leaf growth leading

545

550

to an increase in flow capacities along plant development (Lynn and Carlson, 1990). Until DOY 142, PWU-curves are guided by R_{RX} rather than R_S due to stronger resistance values of the root-xylem system in the early development stages of the winter wheat compared to a sufficiently watered soil for uptake (cf. Figs. 5 & 6). Afterwards, PWU decreased and increased with different strength from DOY 142 until senescence phase (DOY > 190). First, there is a distinct decrease from DOY 142 to DOY 157 (inflorescence and flowering phase, cf. Tab. 1). In this phase the soil moisture dropped mainly due to a daily mean air temperature of about 20 [$°C$] and absence of major precipitation events, leading to a SMP-decrease from -0.03 [MPa] to -0.12 [MPa]. This is accompanied with a significant increase in soil resistance (cf. Fig. 5) and a decrease in root-xylem resistance (cf. Fig. 6).

From DOY 157 to DOY 180 (flowering and grain development phase) rain input was absent and soil water decreased with SMP–values up to -0.2 [MPa] on DOY 180 and a soil conductivity minimum of 1.1×10^{-13} [m/s] (cf. Fig. 5). The VWP-values strongly dropped from -0.28 [MPa] to about -1.75 [MPa]. In this period PWU increased, in the beginning stronger then only slightly, indicating water depletion from the soil (cf. Fig. 9) in the reproductive stage of the wheat plants.

In the last grain development phase (DOY 180 to DOY 190) before senescence (DOY > 190), the VWP further decreased to -2.38 [MPa], but with a milder slope due to refilling water in soils (note that SMP for both soil depths raised to -0.14 [MPa] during several consecutive rain events as seen in Figure 9 as gray bars). The PWU-curves at 5 [cm] depth start to rise again from DOY 191 to DOY 198 due to the first strong rain impulses seen first by the top soil (cf. Fig. 13).

In the senescence phase (DOY 199), the soil moisture was not the limiting factor anymore and VWP dropped to its pre-defined minimum of -2.5 [MPa] as soon as RWC reaches a level of 35 [$\%$], subsequently approaching almost zero beyond DOY 210 (cf. Fig. 11). In Figure 11 a gray-masked area indicates the senescence phase where the water uptake estimates are not valid anymore, since root-xylem resistance is considered to be solely dependent on LAI in (6).

After uptake of water into the wheat plants, we focus in the following on water release from the wheat plants into the atmosphere. In Figure 14, the estimated transpiration rates TR [mm/s] are shown along the growing season including its input variables VWP and VPD. The value range of the TR-estimates is similar to the range presented by Kang et al. 2003 and Zhang et al. 2019 for winter wheat fields, whereby the latter also analyzed different fertilization levels. The general trend of the TR-curves indicates considerable concurrency with the PWU-curves over the entire season in Figure 13. This connection of dynamics, pointing towards steady water flow along the SPAS, supports the connection of the different water storage compartments in the system.

However, the magnitudes of TR and PWU are different especially around the ripening phase of the wheat (around DOY 180) due to differently modelled time-variant flow resistances for both processes. This is more decisive for transpiration (including radiation- and temperature-dependence within VPD) having a stronger diurnal cycle than water uptake (including mainly moisture-dependence within soil matric potential). Hence the temporal dynamics and magnitudes of TR and PWU exhibit no absolute concurrency due to dependence of TR to faster changing atmospheric conditions, while dependence of PWU is on slower changing soil conditions.
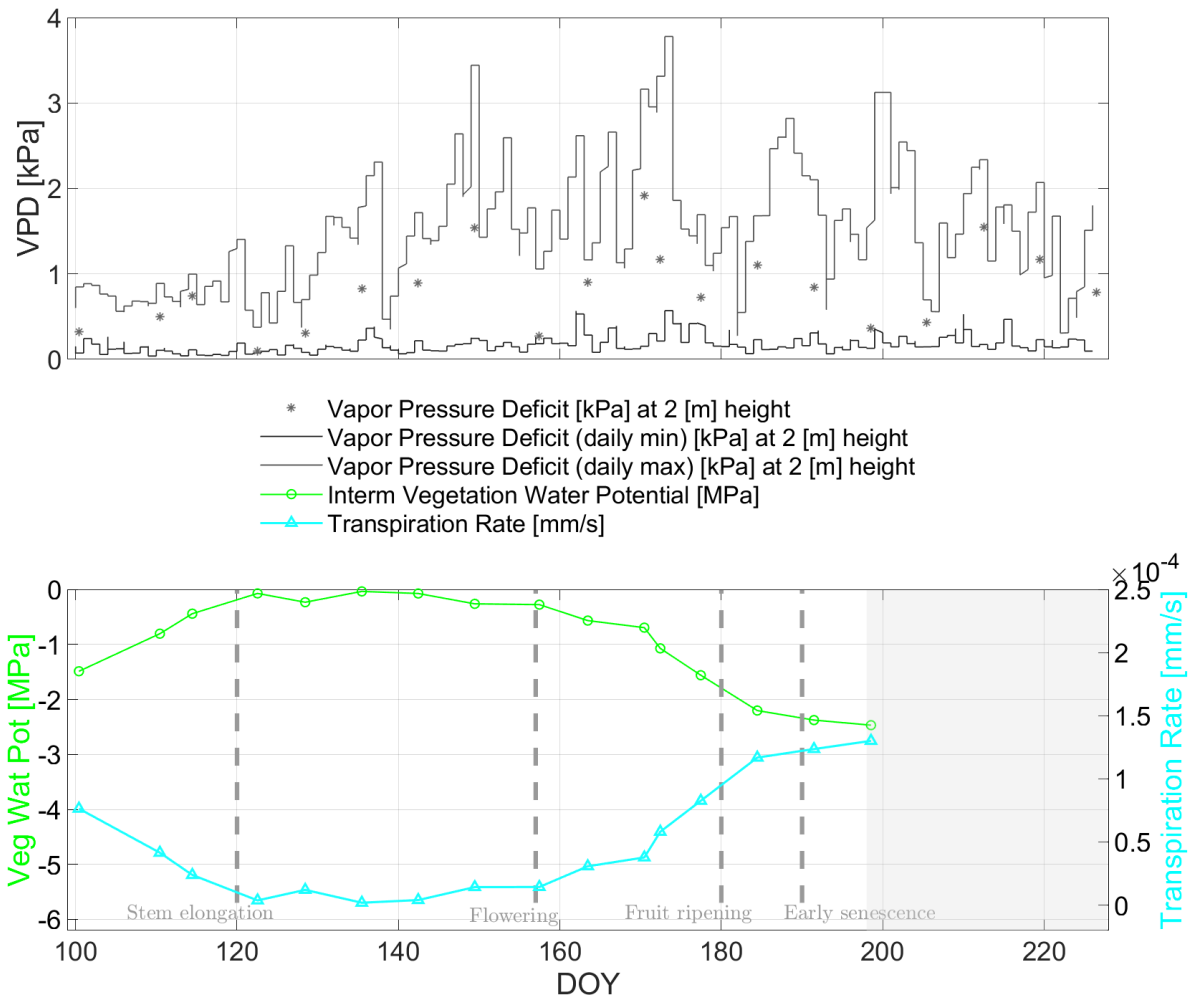
Figure 14: Top: Minimum and maximum of the vapor pressure deficit (VPD) $[kPa]$ for atmospheric water need shown with gray lines. The asterisks indicate the VPD–values at time of radiometer measurement.
Bottom: Comparison of radiometer-based transpiration rates TR $[mm/s]$ (cyan curve for variable canopy & aerodynamic resistances as well as a fixed cuticular resistance) and vegetation water (green curve) potential VWP $[MPa]$ along the growing period of 2017 for days of year (DOY) at the winter wheat field in Selhausen, Germany. The gray-masked area indicates the senescence phase where the assumption in the stomatal resistance calculus is not applicable. Vertical dashed lines indicate major phenological phases of the winter wheat.

Considering both flux estimates, the most interesting part is that for calculating PWU and TR two substantially different in situ measurements (SMP, VPD) were paired together with the same radiometer-based VWP-input. However, the dynamics of both fluxes (PWU, TR) are concurrent in trend and show considerable similarity along

wheat growing season. This comes with the caveat that the applied resistances of the soil-plant-atmosphere compartments were derived from literature (R_C) or form auxiliary in situ information (e.g. soil hydraulic conductivity, leaf area index, net solar radiation and wind speed) applied in empirical models (R_S, R_{RX}, R_{ST}, R_A), (Manzoni et al., 2013b, Monteith & Unsworth, 2013). Nonetheless, VWP as a radiometer-based potential estimate shows considerable similarity in temporal dynamics to the on-site measurement-derived potentials of soil (SMP) and atmosphere (VPD).

For a first comparison with an independent dataset, the estimated transpiration rates of the space-borne ECOSTRESS sensor were used (cf. section 2 for sensor and product characteristics) and shown in Figure 15. Our results show that the value ranges of the ECOSTRESS estimates are equivalent (showing the same order of magnitude) to the field-based TR estimates at Selhausen. In Figure 15 the TR estimates are presented for several years (2017, 2019-2021) and with different sample sizes. Note that the heterogeneity of land surface conditions at the spatial resolution of ECOSTRESS (70 [m]) does not allow for direct validation against the in situ measurements.
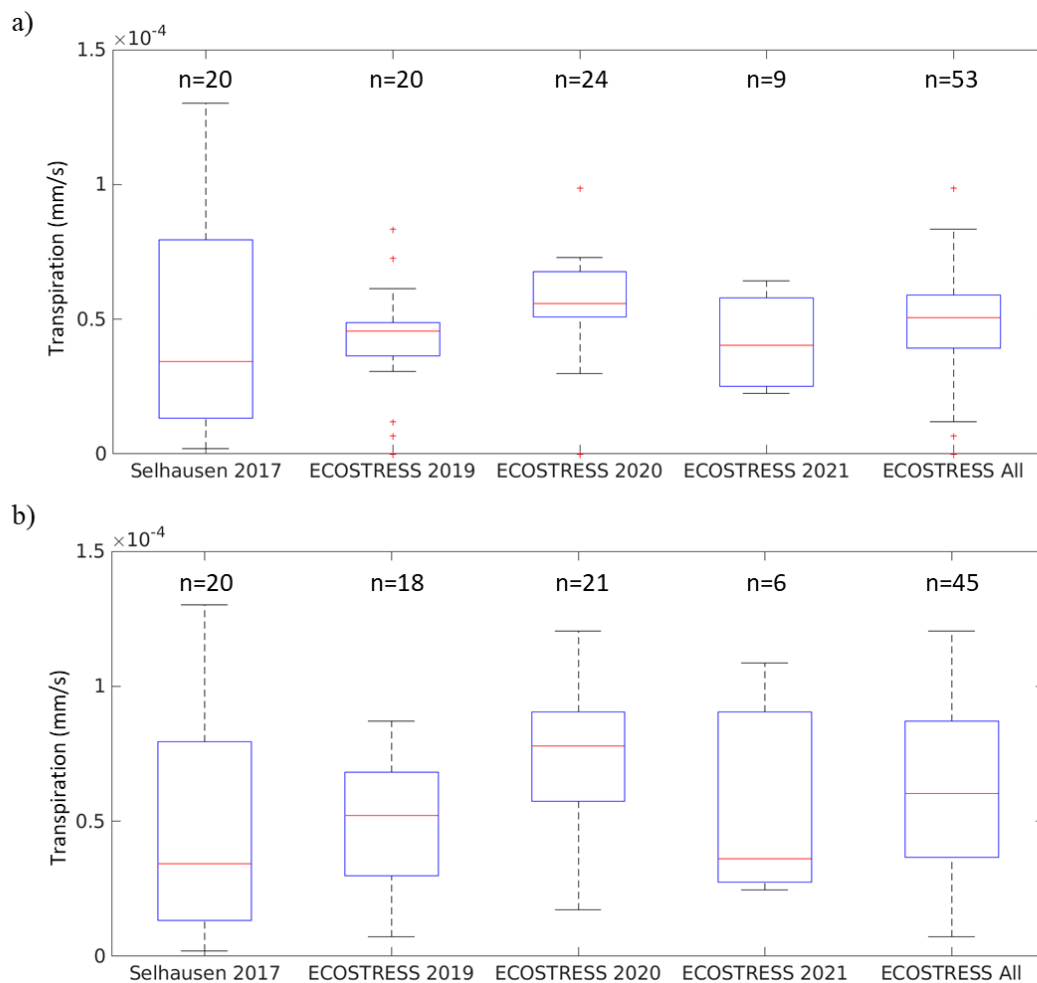
Figure 15: Boxplots of estimated transpiration rates TR $[mm/s]$ comparing the field-based estimates presented for the Selhausen field (see Fig. 14) and (a) the space-borne ECOSTRESS daily product and (b) the instantaneous product. The number of samples (n) is indicated at the top of each box. For each box, the red line shows the median, top and bottom edges are percentiles 75 and 25, respectively, top and bottom whiskers are percentiles 95 and 5, respectively, and red crosses indicate outliers.

5 Discussion

This concept study presents a radiometer-based approach to estimate time-dynamic flux rates (plant water uptake & transpiration) from water status observations along the SPAS, even if assumptions on water flow properties (soil & plant hydraulic traits, e.g. effective soil porosity, rooting depth and flow resistances) and some ancillary data are necessary. With the proposed approach, analyses of the SPAS are enabled covering the different water pools (soil, plant and atmosphere), their potentials (suction tension) and in-between fluxes (uptake, transpiration). The estimates for each water pool are assessible together with a first analysis on how water flows from soil to the atmosphere. Water pools are accessible depending on measurement depth and sensing volume of the in situ and remote sensing sensors. In the case of the soil instruments only the soil moisture and SMP down to 30 [cm] were accessible which may not cover the entire water reservoir from which the wheat roots can take up water. The water may also come from deeper layers. However, White et al. (2015) report that for winter wheat (in 17 experiments) the soil depths of 10 [cm] and 30 [cm] showed a median of the root length density (RLD) above the critical RLD of 1 [$cm\ cm^{-3}$] for wheat.

Interestingly, flux rates of PWU and TR (cf. Figs. 13 & 14) are overall concurrent and similar in trend despite the inclusion of different on-site information in the calculus of fluxes (PWU: Soil permittivity, TR: VPD). This might be a first indication of the feasibility of capturing the continuous water flow within the SPAS by combining radiometer observations and in situ measurements.

In addition, the study relies on snapshot analysis of radiometer-based vegetation parameters (e.g. m_g, RWC and VWP) for single days along the growing period, since radiometer measurements were only conducted over one to two hours within 9 am and 2 pm on a measuring day. No analyses about the diurnal cycle of RWC, VWP, PWU and TR or their sub-daily variability within the wheat canopy can be provided. Thus, all results are representative with respect to their trends along the growing season.

The presented results and first comparison with ECOSTRESS data outline the potential as well as limitations of using passive microwave observations together with on-site information of soil and atmosphere to estimate seasonal water dynamics for a single winter wheat field. As the setup of the experiment at the Selhausen field laboratory is temporally confined (one growing season), specific in setup (metal mesh for soil signal blockage;

only vegetation-related signals included), small-scale (one field) and single-species (only winter wheat), it is at this moment not possible to significantly generalize the presented results with respect to other temporal and spatial domains, species (traits & phenologies) and scales. The generalization of the method is challenging, as for instance,

650   the RWC to VWP conversion (cf. Fig. 3) is plant type-specific and not yet well understood for spatio-temporal resolution conditions of satellite radiometer (passive microwave) remote sensing with resolutions of kilometers in space and days in time (cf. Fig. 2 in Konings et al., 2019). In particular, the conversion from RWC to VWP is semi-empirical. This means the rate and strength of water supply on potential (suction) reduction is not accessible at field scale and along growing season from the on-site measurements, but in a first attempt deducible from

655   literature survey (Turner and Long, 1980; Turner, 1988; Zweifel and Häsler, 2000; Zweifel et al., 2001; Pearcy et al., 2012).

As mentioned above, there are some limitations of the retrieval to arrive from water status at water fluxes. Since effective variables, like the soil, wheat canopy and atmospheric resistances, cannot be directly measured in situ at the field scale, they are estimated by (wheat-specific) mechanistic retrieval models for soil, root-xylem, stomatal

660   and aerodynamic resistances fed with (auxiliary) on-site measurements (cf. sections 3.2 & 3.4 for details). However, the mechanistic models are empirically derived and therefore not complete in terms of their inclusion of all potentially occurring flow resistances within the wheat plants, e.g. intercellular air space resistance. For simplicity the same transpiration from top (adaxial) and bottom (abaxial) side of leaf is assumed (cf. (7) & cf. Nobel, 2020, p.415 and 427ff).

665   Another fundamental specificity of the study setup, mentioned briefly above, is that the soil emission is completely blocked physically by a metal mesh on the ground (ideal investigation conditions for vegetation influence on microwave emission and scattering). This could represent a burden on wide-area monitoring of water dynamics with radiometer-based retrievals. However, a joint approach combining emission modeling and data inversion (e.g. using zeroth- or first-order radiative transfer models (Wigneron et al., 2017)) was used in Meyer et al. (2018) on

670   another part of the wheat field without mesh coverage. Soil and vegetation emission signals were separated leading to equivalent estimates of soil moisture and VOD compared to the values from the mesh-covered part (VOD) and from the in situ measurements (soil moisture). Hence, this might pave the way towards a wide-area retrieval of water dynamics with radiometers at L-band. Algorithms from operating satellite radiometer missions would be available, such as from SMAP (Konings et al., 2017).

675   Despite all restrictions (due to having no complete measurement portfolio of all SPAS variables), no attempts have been reported in literature which follow a similar approach combining soil, plant and atmosphere information from L-band passive radiometry with (on-site) measurements at the field scale. One exception is the correlation of L-band radiometer-derived VOD with water potential measurements of a tree stand at Harvard forest along one growing season (Holtzman et al., 2020). In any case, there is a need for remote sensing-scale analyses of transfer-

680   functions from VOD via water content to water potential in plants, which must be different from laboratory analyses of single tissues of leaves (Turner, 1988).

    In the end, this is a path finder study to water dynamics across winter wheat starting from ground-based L-band radiometry in combination with on-site measurements of soil and atmosphere. Our results show the potential of combining microwave radiometer-based estimates with in situ measurements into crop growth or soil-plant-

685   atmosphere transport models, in agreement with previous studies (Wang and Engel, 2002; Palosuo et al., 2011). Furthermore, atmosphere and soil information, like the VPD or soil moisture, can also be derived today from remote sensing sources, e.g. VPD from Atmospheric Infrared Sounder (AIRS) on-board NASA's Aqua satellite (Feldman et al., 2020) or surface soil moisture from SMAP or SMOS microwave radiometer missions (Entekhabi et al., 2010; Kerr et al., 2010). In addition, a major part of the soil-plant-atmosphere parameters, needed as input

690   in the presented water dynamic calculus and listed in Table 2, can already be estimated today from multi-sensor remote sensing, including lidars (vegetation height), optical sensors (solar net radiation, VPD, LAI), radars/scatterometers (vegetation volume fraction, soil moisture, VOD) and radiometers (VOD, soil moisture,). In this way, the concept study sheds light on a future assessment of the SPAS, solely relying on a combination of multi-sensor remote sensing, preferably on satellite basis. This would enable a wide-area (up to global) assessment

695   of the SPAS in the end. However, this comes with the limitations in spatio-temporal as well as spectral coverage of remote sensing systems, no matter if active (e.g. lidar, radar) or passive (e.g. spectrometer, radiometer) systems are used. Moreover, it has to be acknowledged that remote sensing acquisitions do not purely sense one variable of the earth system, but normally a mixture of variables (e.g. combination of soil and vegetation variables). Hence, the quality of retrieved earth system variables (e.g. soil or plant moisture), extracted from remotely sensed

700   observations, depends directly on the sophistication of the signal-to-variable conversion.

    Moreover, L-band radiometry does not measure fluxes per se. Hence, we need valid estimates of the water reservoirs (soil moisture, plant moisture and relative humidity of atmosphere). Afterwards, we need performant estimates of the water potentials. In the end, we need to transit to the water fluxes, here the essential auxiliaries are

the flow resistances of the soil, vegetation and atmosphere. These resistances are challenging to assess with remote

705   sensing due to multi-factorial (inter-)dependencies. For these reasons, we advocate that in order to retrieve exact

water flow dynamics, a plausible solution may come from the combination of earth system/vegetation growth

models and high spatio-temporal resolution remote sensing data from multiple instruments. This multi-source

approach could be key for applications needing quantitative estimates of water fluxes and will be the subject of

further research.

710   A direct implication of this field-based study is that with more measurements or wider knowledge about plant

characteristics regarding water flux, the approach should be applicable to more plant types and to larger areas

exploiting the wide-area mapping capabilities of space-borne sensors. Future missions, like the Copernicus

Imaging Microwave Radiometer (CIMR) of the European Space Agency (ESA) (Kilic et al., 2018), could be

potential candidates for addressing research on water fluxes within the SPAS on a global scale. This would exploit

715   the benefit of multiple sensing frequencies allowing for different penetration and transmission capabilities through

vegetation canopies (Prigent and Jiménez, 2021; Zhao et al., 2021). Advanced methodologies exploiting the

synergies from present and planned satellite constellations will possibly allow a frequent and large-scale mapping

of water fluxes through the SPAS.

6 Conclusions

720   The objective of this concept study was to investigate whether observations of a ground-based radiometer over a

winter wheat field allow for the estimation of seasonal flux rates of water (plant water uptake and transpiration)

along the soil-plant-atmosphere system (SPAS). We started from L-band radiometry-based vegetation optical depth

(VOD) together with on-site measurements of soil and atmosphere. The major research question behind the

objective was how far L-band radiometry and on-site measurements contain enough information to derive water

725   potentials and flux rates in the SPAS of the winter wheat field along the growing season.

From the presented concept study, first conclusions can be drawn within the boundaries of the experimental setup,

detailed in the former sections. Arriving at exact water fluxes in the SPAS of winter wheat needs further

information (e.g. about soil, plant and atmosphere resistances) than initially acquired during the presented

campaign in 2017 at the Selhausen (Germany) field laboratory. The campaign was originally not designed for

730   studying water fluxes in the SPAS. Existing on-site measurements of soil (permittivity), plant (height & LAI) and

atmosphere (net radiation, temperature & relative humidity of air) were used in the study to estimate water flux rates (PWU & TR). Hence, it is imperative to have water status information (θ, m_g, RH) along the SPAS for estimating water dynamics (cf. Fig. 2). Otherwise, these dynamics cannot be fully assessed. Furthermore, measurements of soil moisture are required from in situ measurements or from estimations based on radiometer observations. In this work we used in situ measurements, which have a higher temporal resolution.

Our concept study outlines possible ways to incorporate L-band radiometry (ground-based remote sensing) in a field-based SPAS assessment. We were able to obtain reasonable estimates of water potentials and water flux rates in the SPAS in terms of the major trend along season. The presented results reveal the capacity of L-band radiometers in combination with in situ measurements to assess water dynamics within the SPAS of a wheat field. A first comparison of TR estimates from the presented field-based approach and from the space-borne ECOSTRESS mission indicates similar value ranges (same order of magnitude). However, the validation of absolute accuracies needs to be tackled in future studies with dedicated in situ measurements of water dynamics (potentials & flux rates).

This concept study sheds light on the potential of radiometer-integrated SPAS research. Our proposed approach should be further explored with dedicated field laboratory studies, explicitly including ground-based (L-band) radiometry and other remote sensing sensors together with in situ measurements necessary to validate water flux dynamics, such as soil water potential, leaf water potential, sap flux, stomatal conductance and transpiration rates. Based on the initial results of this study, we advocate that a hybrid-based (remote sensing & earth system models), wide-area (up to global) SPAS assessment could potentially be established in the future.

Acknowledgments. The authors thank Dr. Andrew Feldman (MIT), Prof. Dr. Dara Entekhabi (MIT), Dr. Stan Schymanski (LIST) and Prof. Dr. Jordi Martínez-Vilalta (CREAF) for their helpful comments and suggestions supporting this research. They also thank Mr. Mark Lützner for language editing. The authors want to acknowledge MIT for supporting this research with the MIT-Germany Seed Fund "Global Water Cycle and Environmental Monitoring using Active and Passive Satellite-based Microwave Instruments" and with the MIT-Belgium UCL Seed Fund "Early Detection of Plant Water Stress Using Remote Sensing". The ELBARA-II radiometer was provided by the Terrestrial Environmental Observatories (TERENO) initiative funded by the Helmholtz Association of German Research Centers. D.C. has received funding by "la Caixa" Foundation (ID 100010434), under agreement LCF/PR/MIT19/51840001, by the MIT-MISTI, and by the Spanish government through projects ESP2017-89463-C3-2-R, RTI2018-096765-A-I00 and MDM-2016-0600.

Author Contributions. Conceptualization, T.J., F.J. and M.P.; Methodology, T.J., A.F., F.J., D.C. and M.P.; Software, T.J., F.J., A.F. and T.M.; Formal Analysis, All; Data Curation, T.M., F.J., T.J. and A.F.; Writing-Original Draft Preparation, T.J., A.F., F.J., D.C., M.J.B. and M.P.; Writing-Review & Editing, All; Visualization, T.J., A.F., F.J., M.J.B. and T.M.; Supervision, M.P..

Data availability. All data were recorded by Forschungszentrum Jülich, Institute of Bio- and Geosciences, Agrosphere (IGB-3), and are partly available upon request from François Jonard (f.jonard@fz-Juelich.de). TERENO data are available at www.tereno.net. ECOSTRESS datasets are freely available at https://ecostress.jpl.nasa.gov/data/.

Competing interests. The authors declare that they have no conflict of interest.

770

References

Alduchov, O. A., and Eskridge, R. E.: Improved Magnus form approximation of saturation vapor pressure, Journal of applied meteorology, 35(4), 601-609, 1996.

Allen, R. G., Pereira, L. S., Raes, D., and Smith, M.: Crop evapotranspiration-Guidelines for computing crop water
775 requirements-FAO Irrigation and drainage paper 56, FAO, Rome, 300(9), D05109, 1998.

Blizzard, W.E. and Boyer, J.S.: Comparative resistance of the soil and the plant to water transport. Plant physiology, 66(5), 809-814, 1980.

Bonan, G. B., Williams, M., Fisher, R. A., and Oleson, K. W.: Modeling stomatal conductance in the earth system: linking leaf water-use efficiency and water transport along the soil–plant–atmosphere continuum. Geoscientific
780 Model Development, 7(5), 2193-2222, 2014.

Brooks, R.H. and Corey, A.T.: Properties of porous media affecting fluid flow, in J. Irrig. Drain. Div. 92, 61–90, 1964.

Bruns, H.A., and Croy, L.I.: Key developmental stages of winter wheat, Triticum aestivum. Economic botany, 37(4), 410-417, 1983.

785 Cai, G., Vanderborght, J., Langensiepen, M., Schnepf, A., Hüging, H. and Vereecken, H.,: Root growth, water uptake, and sap flow of winter wheat in response to different so,il water conditions. Hydrology and Earth System Sciences, 22(4), 2449-2470, 2018.

Campbell, G.: A simple method for determining unsaturated conductivity from moisture retention data, in Soil Sci., 117, 311-314, 1974.

790 Castellvi, F., Perez, P.J., Villar, J.M. and Rosell, J.I.: Analysis of methods for estimating vapor pressure deficits and relative humidity, Agricultural and Forest Meteorology, 82(1-4), 29-45, 1996.

Choat, B., Brodribb, T. J., Brodersen, C. R., Duursma, R. A., López, R., and Medlyn, B. E.: Triggers of tree mortality under drought, Nature, 558(7711), 531-539, 2018.

Choudhury, B.J. and Idso, S.B.: An empirical model for stomatal resistance of field-grown wheat, Agricultural and
795 forest meteorology, 36(1), 65-82, 1985.

Choudhury, B. J., and Idso, S. B.: Evaluating plant and canopy resistances of field-grown wheat from concurrent diurnal observations of leaf water potential, stomatal resistance, canopy temperature, and evapotranspiration flux, Agricultural and forest meteorology, 34(1), 67-76, 1985.

Clapp, R.B. and Hornberger, G.M.: Empirical equations for some soil hydraulic properties, in Water Resour. Res. 14, 601–604, 1978.

Cowan, I. R.: Transport of water in the soil-plant-atmosphere system, Journal of Applied Ecology, 221-239, 1965.

Curtis, B. C., Rajaram, S., and Gómez Macpherson, H.: Bread wheat: improvement and production. Food and Agriculture Organization of the United Nations (FAO), report, 2002.

Damour, G., Simonneau, T., Cochard, H., and Urban, L.: An overview of models of stomatal conductance at the leaf level, Plant, Cell and Environment, 33(9), 1419-1438, 2010.

Dingman, S. L.: Physical hydrology. Waveland Press, Long Grove, USA, 2015.

Duursma, R. A., Blackman, C. J., Lopéz, R., Martin-StPaul, N. K., Cochard, H., and Medlyn, B. E.: On the minimum leaf conductance: its role in models of plant water use, and ecological and environmental controls, New Phytologist, 221(2), 693-705, 2019.

Eamus, D., Huete, A., and Yu, Q.: Vegetation dynamics, Cambridge University Press, U.K., 2016.

Elfving, D.C., Kaufmann, M.R., and Hall, A.E.: Interpreting leaf water potential measurements with a model of the soil-plant-atmosphere continuum, Physiologia plantarum, 27(2), 161-168, 1972.

Entekhabi, D., Njoku, E. G., O'Neill, P. E., Kellogg, K. H., Crow, W. T., Edelstein, W. N., et al.: The soil moisture active passive (SMAP) mission, Proceedings of the IEEE, 98(5), 704-716, 2010.

Fan, J., McConkey, B., Wang, H., and Janzen, H.: Root distribution by depth for temperate agricultural crops, Field Crops Research, 189, 68-74, 2016.

Feddes, R. A., and Rijtema, P. E.: Water withdrawal by plant roots, Journal of Hydrology, 17(1-2), 33-59, 1972.

Feldman, A.F., Short Gianotti, D.J., Trigo, I.F., Salvucci, G.D. and Entekhabi, D.: Land-atmosphere drivers of landscape-scale plant water content loss, Geophysical Research Letters: Hydrology and Land Surface Studies, DOI: 10.1029/2020GL090331, 2021.

Fink, A., Jagdhuber, T., Piles, M., Grant, J., Baur, M., Link, M., and Entekhabi, D.: Estimating Gravimetric Moisture of Vegetation Using an Attenuation-Based Multi-Sensor Approach, In IGARSS 2018-2018 IEEE International Geoscience and Remote Sensing Symposium (353-356). IEEE, 2018.

Frank, A. B., Power, J.F., and Willis, W.O.: Effect of Temperature and Plant Water Stress on Photosynthesis, Diffusion Resistance, and Leaf Water Potential in Spring Wheat, Agronomy journal, 65(5), 777-780, 1973.

Gallardo, M., Eastham, J., Gregory, P.J. and Turner, N.C.: A comparison of plant hydraulic conductances in wheat and lupins, Journal of Experimental Botany, 47(2), 233-239, 1996.

Gardner, W. R.: Dynamic aspects of water availability to plants, Soil science, 89(2), 63-73, 1960.

Gardner, W. R.: Dynamic aspects of soil-water availability to plants, Annual review of plant physiology, 16(1), 323-342, 1965.

Gupta, A. S., Berkowitz, G. A., and Pier, P. A.: Maintenance of photosynthesis at low leaf water potential in wheat: role of potassium status and irrigation history, Plant Physiology, 89(4), 1358-1365, 1989.

Gupta, S.C. and Wang, D.: Water Retention in Soil, in Encyclopedia of Soil Science, R. Lal (Ed.), CRC Press, Taylor and Francis Group, Boca Raton, FL, USA, ISBN: 9780849350542, 2006.

Halverson, G.H., Fisher, J.B., and Lee, C.M.: ECOsystem Spaceborne Thermal Radiometer Experiment on Space Station (ECOSTRESS). Mission Level 3 Evapotranspiration Priestley-Taylor Jet Propulsion Laboratory (PT-JPL), Data User Guide D-57153, Version 2, Jet Propulsion Laboratory, California Institute of Technology. Pasadena, CA, United States, 1-18, 2019.

Hillel, D. Fundamentals of soil physics, Academic Press. New York, 1980.

Holtzman, N., Anderegg, L.D.L., Kraatz, S., Mavrovic, A., Sonnentag, O., Pappas, C., Cosh, M.H., Langlois, A., Lakhankar, T., Tesser, D., Steiner, N., Colliander, A., Roy, A., and Konings, A.G.: L-band vegetation optical depth as an indicator of plant water potential in a temperate deciduous forest stand, Biogeosciences, 18, 739-753, 2021.

Johnson, K. M., Jordan, G. J., and Brodribb, T. J.: Wheat leaves embolized by water stress do not recover function upon rewatering, Plant, Cell and Environment, 41(11), 2704-2714, 2018.

Jonard, F., Weihermüller, L., Schwank, M., Jadoon, K. Z., Vereecken, H., and Lambot, S.: Estimation of hydraulic properties of a sandy soil using ground-based active and passive microwave remote sensing, IEEE transactions on geoscience and remote sensing, 53(6), 3095-3109, 2015.

Jonard, F., Bircher, S., Demontoux, F., Weihermüller, L., Razafindratsima, S., Wigneron, J. P., and Vereecken H.: Passive L-band microwave remote sensing of organic soil surface layers: a tower-based experiment, Remote Sensing, 10(2), 304, 2018.

Jonard F., De Cannière S., Brüggemann N., Gentine P., Short Gianotti D. J., Lobet G., Miralles D. J., Montzka C., Pagán B. R., Rascher U., and Vereecken H.: Value of chlorophyll fluorescence for quantifying hydrological states and fluxes: Current status and challenges, Agricultural and Forest Meteorology, 291: 108088. https://doi.org/10.1016/j.agrformet.2020.108088, 2020.

Kameli, A., and Lösel, D. M.: Carbohydrates and water status in wheat plants under water stress, New Phytologist, 125(3), 609-614, 1993.

Kang, S., Gu, B., Du, T., and Zhang, J.: Crop coefficient and ratio of transpiration to evapotranspiration of winter wheat and maize in a semi-humid region. Agricultural water management, 59(3), 239-254, 2003.

Kerr, Y. H., Waldteufel, P., Wigneron, J. P., Delwart, S., Cabot, F., Boutin, J., et al.: The SMOS mission: New tool for monitoring key elements of the global water cycle, Proceedings of the IEEE, 98(5), 666-687, 2010.

Kilic, L., et al.: Expected performances of the Copernicus Imaging Microwave Radiometer (CIMR) for an all-weather and high spatial resolution estimation of ocean and sea ice parameters, Journal of Geophysical Research: Oceans 123.10, 7564-7580, 2018.

Konings, A. G., Piles, M., Das, N., and Entekhabi, D.: L-band vegetation optical depth and effective scattering albedo estimation from SMAP, Remote Sensing of Environment, 198, 460-470, 2017.

Konings, A. G., Rao, K., and Steele-Dunne, S. C.: Macro to micro: microwave remote sensing of plant water content for physiology and ecology, New Phytologist, 223(3), 1166-1172, 2019.

Lambers, H., Stuart Chapin III, F., and Pons T.L.: Plant physiological ecology, Springer Science and Business Media, 2008.

Lynn, B. H., and Carlson, T. N.: A stomatal resistance model illustrating plant vs. external control of transpiration, Agricultural and Forest Meteorology, 52(1-2), 5-43, 1990.

Mätzler, C.: Microwave (1–100 GHz) dielectric model of leaves. IEEE Trans. Geosci. Remote Sens., 32, 947–949, 1994.

Manzoni, S., Vico, G., Porporato, A., and Katul, G.: Biological constraints on water transport in the soil–plant–atmosphere system, Advances in Water Resources, 51, 292-304, 2013a.

Manzoni, S., Vico, G., Katul, G., Palmroth, S., Jackson, R. B., and Porporato, A.: Hydraulic limits on maximum plant transpiration and the emergence of the safety–efficiency trade-off, New Phytologist, 198(1), 169-178, 2013b.

Manzoni, S., Vico, G., Katul, G., Palmroth, S., and Porporato, A.: Optimal plant water-use strategies under stochastic rainfall, Water Resources Research, 50(7), 5379-5394, 2014.

Margulis, S. A.: Introduction to hydrology, https://ucla.app.box.com/v/Intro-to-Hydrology-pdf, 2017.

Martínez-Vilalta, J., and Garcia-Forner, N.: Water potential regulation, stomatal behaviour and hydraulic transport under drought: deconstructing the iso/anisohydric concept, Plant, Cell and Environment, 40(6), 962-976, 2017.

Martinez-Vilalta, J., Anderegg, W. R., Sapes, G., and Sala, A.: Greater focus on water pools may improve our ability to understand and anticipate drought-induced mortality in plants, New Phytologist, 2019.

Matheny, A. M., Mirfenderesgi, G., and Bohrer, G.: Trait-based representation of hydrological functional properties of plants in weather and ecosystem models, Plant diversity, 39(1), 1-12, 2017.

Meyer, T., Weihermüller, L., Vereecken, H., and Jonard, F.: Vegetation Optical Depth and Soil Moisture Retrieved from L-Band Radiometry over the Growth Cycle of a Winter Wheat, Remote Sensing, 10(10), 1637, 2018.

Meyer, T., Jagdhuber, T., Piles, M., Fink, A., Grant, J., Vereecken, H., and Jonard, F.: Estimating Gravimetric Water Content of a Winter Wheat Field from L-Band Vegetation Optical Depth. Remote Sensing, Remote Sensing 11(20), 2353, 2019.

895   Momen, M., and Bou-Zeid, E.: Analytical reduced models for non-stationary diabatic atmospheric boundary layers, Boundary-Layer Meteorology, 164(3), 383–399. https://doi.org/10.1007/s10546-017-0247-0, 2017.

Momen, M., Wood, J. D., Novick, K. A., Pangle, R., Pockman, W. T., McDowell, N. G., and Konings, A. G.: Interacting effects of leaf water potential and biomass on vegetation optical depth, Journal of Geophysical Research: Biogeosciences, 122(11), 3031-3046, 2017.

Monteith, J. L.: Evaporation and environment. In Symposia of the society for experimental biology, 19, 205-234. 900   Cambridge University Press (CUP) Cambridge, 1965.

Monteith, J., and Unsworth, M.: Principles of environmental physics: plants, animals, and the atmosphere. Academic Press. Cambridge, USA, 2013.

Nobel, P.S.: Physicochemical and Environmental Plant Physiology, Academic Press. Cambridge, USA, 2020.

Oosterhuis, D. M., and Walker, S.: Stomatal resistance measurement as an indicator of water deficit stress in wheat 905   and soybeans, South African Journal of Plant and Soil, 4(3), 113-120, 1987.

Palosuo, T., Kersebaum, K. C., Angulo, C., Hlavinka, P., Moriondo, M., Olesen, J. E., et al.: Simulation of winter wheat yield and its variability in different climates of Europe: a comparison of eight crop growth models, European Journal of Agronomy, 35(3), 103-114, 2011.

Passioura, J. B.: Water in the soil-plant-atmosphere continuum, In Physiological plant ecology II (5-33). Springer, 910   Berlin, Heidelberg, 1982.

Pearcy, R. W., Ehleringer, J. R., Mooney, H., and Rundel, P. W. (Eds.). Plant physiological ecology: field methods and instrumentation, Springer Science and Business Media, 2012.

Portal, G., Jagdhuber, T., Vall-llossera, M., Camps, A., Pablos, M., Entekhabi, D., and Piles, M.: Assessment of Multi-Scale SMOS and SMAP Soil Moisture Products across the Iberian Peninsula, Remote Sensing, 12(3), 570, 915   2020.

Prigent, C., and Jimenez, C.: An evaluation of the synergy of satellite passive microwave observations between 1.4 and 36 GHz, for vegetation characterization over the Tropics, Remote Sensing of Environment, 257, 112346, 2021.

Rao, K., Anderegg, W. R., Sala, A., Martínez-Vilalta, J., and Konings, A. G.: Satellite-based vegetation optical 920   depth as an indicator of drought-driven tree mortality, Remote Sensing of Environment, 227, 125-136, 2019.

Rascio, A., Platani, C., Scalfati, G., Tonti, A., and Di Fonzo, N.: The accumulation of solutes and water binding strength in durum wheat, Physiologia Plantarum, 90(4), 715-721, 1994.

Reichardt, K., and Timm, L. C.: Soil, plant and atmosphere, Springer Nature Switzerland, Cham, Switzerland, 2014.

925   Ritchie, J. T.: Water dynamics in the soil-plant-atmosphere system, Plant and Soil, 81-96, 1981.

Ruggiero, C., Angelino, G., Maggio, A.: Developmental regulation of water uptake in wheat, Journal of Plant Physiology, 164, 1170-1178, 2007.

Sadeghi, M., Gao, L., Ebtehaj, A., Wigneron, J. P., Crow, W. T., Reager, J. T., and Warrick, A. W.: Retrieving global surface soil moisture from GRACE satellite gravity data, Journal of Hydrology, 584, 124717, 2020a.

930   Sadeghi, M., et al.: Global estimates of land surface water fluxes from SMOS and SMAP satellite soil moisture data, Journal of Hydrometeorology 21.2, 241-253, 2020b.

Sarto, M. V., M., Sarto, J. R. W., Rampim, L., Rosset, J. S., Bassegio, D., da Costa, P. F., and Inagaki, A. M.: Wheat phenology and yield under drought: a review, *Australian Journal of Crop Science*, *11*(8), 941, 2017.

Schmugge, T.J and; Jackson, T.J.: A dielectric model of the vegetation effects on the microwave emission from 935   soils, IEEE Trans. Geosci. Remote Sens., 30, 757–760, 1992.

Shukla, M.K.: Soil physics. An Introduction, CRC Press, Taylor and Francis Group, Boca Raton, FL, USA, ISBN: 9781439888421, 2014.

Siddique, M. R. B., Hamid, A. I. M. S., and Islam, M. S.: Drought stress effects on water relations of wheat, Bot. Bull. Acad. Sin, 41(1), 35-39, 2000.

940   Slatyer, R. O., and Taylor, S. A.: Terminology in plant-and soil-water relations, Nature, 187(4741), 922-924, 1960.

Smart, R. E., and Bingham, G. E.: Rapid estimates of relative water content, Plant physiology, 53(2), 258-260, 1974.

Steduto, P., Hsiao, T. C., Fereres, E., and Raes, D.: Crop yield response to water, Rome: Food and Agriculture Organization of the United Nations, report, 1028, 2012.

945   Steenpass, C., Vanderborght, J., Herbst, M., Šimůnek, J., and Vereecken, H.: Estimating soil hydraulic properties from infrared measurements of soil surface temperatures and TDR data, Vadose zone journal, 9(4), 910-924, 2010.

Topp, G.C., Davis, J.L. and Annan, A.P.: Electromagnetic determination of soil water content: measurements in coaxial transmission lines, in Water Resources Research, 1 6(3), 574-582, DOI: [10.1029/WR016i003p00574](10.1029/WR016i003p00574), 1980.

950   Turner, N. C., and Long, M. J.: Errors arising from rapid water loss in the measurement of leaf water potential by the pressure chamber technique, Functional Plant Biology, 7(5), 527-537, 1980.

Turner, N. C.: Measurement of plant water status by the pressure chamber technique, Irrigation science, 9(4), 289-308, 1988.

Tyree, M. T., and Zimmermann, M. H.: Xylem structure and the ascent of sap, Springer Science and Business Media, 2013.

Ulaby, F. and El-Rayes, M.: Microwave dielectric spectrum of vegetation—Part II: Dual-dispersion model, IEEE Trans. Geosci. Remote Sens., 5, 550–557, 1987.

Van den Honert, T. H.: Water transport in plants as a catenary process, Discussions of the Faraday Society, 3, 146-153, 1948.

van Genuchten, M.T.: A Closed-form Equation for Predicting the Hydraulic Conductivity of Unsaturated Soils, in Soil Science Society of America Journal, 44, 892-898, DOI:10.2136/sssaj1980.03615995004400050002x, 1980.

Wallace, J. S.: Water transport and leaf water relations in winter wheat crops, Doctoral dissertation, University of Nottingham, 1978.

Wallace, J. S., and Biscoe, P. V.: Water relations of winter wheat: 4. Hydraulic resistance and capacitance in the soil-plant system, The Journal of Agricultural Science, 100(3), 591-600, 1983.

Wang, E., and Engel, T.: Simulation of growth, water and nitrogen uptake of a wheat crop using the SPASS model, Environmental Modelling and Software, 17(4), 387-402, 2002.

Ward, R. C., and Robinson, M. Principles of hydrology, 3rd edition. McGraw-Hill, London, 2014.

White, C. A., Sylvester-Bradley, R., and Berry, P. M.: Root length densities of UK wheat and oilseed rape crops with implications for water capture and yield. Journal of Experimental Botany, 66(8), 2293-2303, 2015.

Wigneron, J-P., et al.: Modelling the passive microwave signature from land surfaces: A review of recent results and application to the L-band SMOS and SMAP soil moisture retrieval algorithms, Remote Sensing of Environment, 192, 238-262, 2017.

Xu, Xiangtao, Konings, A. G., Longo, M., Feldman, A., Xu, L., Saatchi, S., Wu, D., Wu, J. and Moorcroft, P.: Leaf surface water, not plant water stress, drives diurnal variation in tropical forest canopy water content, New Phytologist, 231, 122-136, 2021.

Yang, S. J., and Jong, E. D.: Effect of soil water potential and bulk density on water uptake patterns and resistance to flow of water in wheat plants, Canadian Journal of Soil Science, 51(2), 211-220, 1971.

Zhang, T., Hou, M., Liu, L.,d and Tian, F.: Estimation of transpiration and canopy cover of winter wheat under different fertilization levels using thermal infrared and visible imagery. Computers and Electronics in Agriculture, 165, 104936, 2019.

Zhao, T., Shi, J., Entekhabi, D., Jackson, T. J., Hu, L., Peng, Z., et al.: Retrievals of soil moisture and vegetation optical depth using a multi-channel collaborative ddalgorithm, Remote Sensing of Environment, 257, 112321, 2021.

985 Zweifel, R. and Häsler, R.: Stem radius changes and their relation to stored water in stems of young Norway spruce trees, Trees, 15(1), 50-57, 2000.

Zweifel, R., Item, H., and Häsler, R.: Link between diurnal stem radius changes and tree water relations, Tree physiology, 21(12-13), 869-877, 2001.